Grid connection of offshore renewable energy sources

Christoffer Fjellstedt

UPPSALA
UNIVERSITET

Dissertation presented at Uppsala University to be publicly examined in Heinz-Otto Kreiss, Ångströmlaboratoriet, Lägerhyddsvägen 1, Uppsala, Friday, 3 March 2023 at 10:00 for the degree of Licentiate of Technology. The examination will be conducted in English. Faculty examiner: Docent Daniel Månsson (Kungliga Tekniska Högskolan (KTH)).

Abstract
Fjellstedt, C. 2023. Grid connection of offshore renewable energy sources. 61 pp. Uppsala: Department of Electrical Engineering.

In order to achieve net zero emissions from the electricity sector, the proportion of renewable energy sources connected to the electrical grid needs to be increased significantly in the coming years. Established renewable energy sources, such as wind power and solar power, will certainly be crucial in achieving this. However, marine energy sources, like marine current power and wave power, have the potential to significantly contribute to the increase of electricity from renewable energy. An important area of study to enable the use of marine energy sources is how to construct electrical systems for offshore renewable energy. Therefore, this thesis addresses some challenges regarding the grid connection of offshore renewable energy.

Two important questions for offshore renewable energy are how the offshore electrical grid is constructed and how the power is transmitted to the shore. In the thesis, a review of AC and DC collection grid topologies is presented. Furthermore, HVAC and HVDC transmission for offshore applications are compared in a literature review. It is concluded that for transmission distances longer than 50 km to 100 km, the preferred technology appears to be HVDC.

Regardless of how the offshore collection grid is constructed, the energy converters need to be connected to the collection grid and the distribution grid. Uppsala University has deployed a marine current energy converter in the river Dalälven in Söderfors, Sweden. The electrical grid connection system at the test site is based on a B2B converter technology. In the thesis, a simulation model of the grid connection system of the energy converter is presented.

The grid connection system at the Söderfors test site includes an LC-filter connected to a power transformer. A novel transfer function is derived for this system and the transfer function is verified with simulations and experimental investigations. It is shown that the derived transfer function is able to capture the frequency response of the experimental system.

Keywords: Grid connection, Electronic filters, Power transformers, Offshore collection grids, HVDC transmission, HVAC transmission, Marine current energy

Christoffer Fjellstedt, Department of Electrical Engineering, Electricity, Box 65, Uppsala University, SE-751 03 Uppsala, Sweden.

URN urn:nbn:se:uu:diva-496087 (http://urn.kb.se/resolve?urn=urn:nbn:se:uu:diva-496087)

”No plan of operations reaches with any certainty beyond the first encounter with the enemy’s main force”
Helmuth von Moltke (1800-1891)

List of papers

This thesis is based on the following papers, which are referred to in the text by their Roman numerals.

I **Fjellstedt, C.**, Forslund, J., Thomas, K., ”Simulations of the electrical system of a grid connected marine current energy converter”, *Proceedings of the 14th European Wave and Tidal Energy Conference (EWTEC)*, 5-9th September, 2021, Plymouth, UK.

II **Fjellstedt, C.**, Ullah, M.I., Forslund, J., Jonasson, E., Temiz, I., Thomas, K., ”A Review of AC and DC Collection Grids for Offshore Renewable Energy with a Qualitative Evaluation for Marine Energy Resources”, *Energies* 2022, 15(16), 5816.

III **Fjellstedt, C.**, Forslund, J., Thomas, K., ”Experimental investigation of the frequency response of an LC-filter and power transformer for grid connection”, Manuscript submitted to the International Journal of Electrical Power & Energy Systems, 2023.

Contents

List of symbols

The list of symbols is for the comprehensive summary. The papers may use other symbols.

Symbol	Unit	Quantity
C	F	Capacitor
C_f	F	Filter capacitor
f_0	Hz	Resonance frequency
H_L	Ω^{-1}	Transfer function of L-filter
H_{LC}	-	Transfer function of LC-filter
H_{LCL}	Ω^{-1}	Transfer function of LCL-filter
H_{LCT}	Ω^{-1}	Transfer function of LC-filter and power transformer model
H_{LCTr}	Ω^{-1}	Reduced and lossless transfer function of LC-filter and power transformer model
I_C	A	Current in a capacitor
I_g	A	Grid current
I_{in}	A	Input current to a filter
I_{out}	A	Output current from a filter
I_1	A	Primary side current in an ideal transformer
I_2	A	Secondary side current in an ideal transformer
i_{as}	A	Phase a current of the generator (similar for phase b and c)
i_{DC}	A	Current transmitted to the shore from a parallel DC collection grid with offshore connection point
i_{dc}	A	Current from one parallel DC collection grid
i_{dg}	A	dq-frame component of grid currents
i^*_{dg}	A	Reference d-component of grid currents
i_{do}	A	Current from one energy converter in a parallel DC collection grid
i_{ds}	A	dq-frame component of generator currents
i^*_{ds}	A	Reference d-component of the generator currents
i_{qg}	A	dq-frame component of grid currents
i_{qs}	A	dq-frame component of generator currents
L	H	Inductor
L_m	H	Magnetizing inductance of the transformer
L_p	H	Primary side leakage inductance of the transformer
L_s	H	Secondary side leakage inductance of the transformer
L_1	H	Inductor in L-filter, LC-filter and LCL-filter
L_2	H	Second inductor in LCL-filter
N_1	-	Number of turns in the primary winding in the transformer

Continued on next page

N_2	-	Number of turns in the secondary winding in the transformer
n	-	Turns ratio
P_g	W	Active power exchanged with the grid
p	-	Number of pole pairs
r	m	Turbine radius
T_e	Nm	Electromagnetic torque
V_{in}	V	Input voltage to a filter
V_{out}	V	Output voltage from a filter
V_1	V	Primary side voltage of the ideal transformer
V_2	V	Secondary side voltage of the ideal transformer
v_{DC}	V	Transmission voltage for series DC collection grid
v_{dc}	V	DC-link voltage
v_{dc}^*	V	Reference value for the DC-link voltage
v_{di}	V	dq-frame component of grid side converter voltages
v_{di}^*	V	Reference d-component of grid side converter voltages
v_{dg}	V	dq-frame component of grid voltages
v_{do}	V	Voltage from one energy converter in a series DC collection grid
v_{ds}	V	dq-frame component of generator voltages
v_{ds}^*	V	Reference d-component of generator voltages
v_{qg}	V	dq-frame component of grid voltages
v_{qi}	V	dq-frame component of grid side converter voltages
v_{qi}^*	V	Reference q-component of grid side converter voltages
v_{qs}	V	dq-frame component of generator voltages
v_w	m/s	Water speed
Q_g	var	Reactive power exchanged with the grid
Q_g^*	var	Reference value for the reactive power exchanged with the grid
R_c	Ω	Resistance representing the core losses in the transformer
R_p	Ω	Primary side winding resistance in the transformer
R_s	Ω	Secondary side winding resistance in the transformer
Z_L	Ω	Impedance of an inductor
Z_{L_m}	Ω	Impedance of the magnetizing inductance in the transformer
Z_p	Ω	Impedance of the primary side series components in the transformer
Z_{R_C}	Ω	Impedance of the core resistance in the transformer
θ_e	rad	Electrical angle of the generator
θ_g	rad	Grid voltage angle
λ	-	Tip speed ratio
λ_{opt}	-	Optimal tip speed ratio
ψ_r	Wb	Rotor flux linkage
ω_e	rad/s	Electrical angular frequency of the generator
ω_g	rad/s	Angular frequency of the grid voltages
$\omega_{res,LC}$	rad/s	Resonance frequency of a lossless LC-filter
$\omega_{res,LCL}$	rad/s	Resonance frequency of a lossless LCL-filter
ω_t	rad/s	Angular velocity of the turbine
$\omega_{t,ref}$	rad/s	Reference angular velocity of the turbine

List of abbreviations

Abbreviation	Meaning
AC	Alternating Current
B2B	Back-to-Back
DC	Direct Current
FOC	Field-Oriented Control
HVAC	High-Voltage Alternating Current
HVDC	High-Voltage Direct Current
IEA	International Energy Agency
MPPT	Maximum Power Point Tracking
PCC	Point of Common Coupling
PMSG	Permanent Magnet Synchronous Generator
PWM	Pulse-Width Modulation
TSO	Transmission System Operator
2L-VSC	2-Level Voltage Source Converter
3L-VSC	3-Level Voltage Source Converter

1. Introduction

In this chapter, a background to the thesis is first presented. Afterwards, the aim and outline of the thesis are given, and finally marine current power research at the Division of Electricity at Uppsala University is discussed.

1.1 Background

The demand for renewable energy is growing, and in 2021 the global renewable power capacity additions increased by 17 %, which corresponds to an added capacity of more than 314 GW [1]. According to a road map set out by the International Energy Agency (IEA) to achieve net zero emission from the energy sector by 2050, annual renewable power capacity additions need to increase to almost 1200 GW by 2030 and on average stay above 1050 GW from 2031 to 2050 [2]. Established renewable energy sources, such as wind power and solar power, will most certainly have a crucial role in achieving the increase in electricity from renewable energy. However, marine energy sources, like marine currents and waves, also have the potential to contribute to the net zero goal. In [3], a theoretical global potential of wave energy of 32 PWh/year is reported, and in [4], global estimates in the range from 0.146 PWh/year to 29.5 PWh/year are reported. The global potential of marine currents has not been investigated to the same extent but in [3], a global estimate of 3 TW is reported. Even though marine energy has a large potential, it still only constitutes a very small part of the global renewable energy market. In 2021 the installed global capacity was only around 524 MW, where the main contribution was from two tidal range systems [1]. The large potential and low utilization of marine energy sources make it a very interesting research area.

For offshore renewable energy, the question of how to construct the electrical grid becomes important when multiple energy converters are considered. The trend in offshore wind power is towards large wind farms located far from the shore [5, 6]. At a certain transmission distance and size of the farm, it can become necessary to transmit the power to the shore using high-voltage direct current (HVDC) [7]. Even if HVDC is used for the transmission to the shore, the internal collection grid in the wind farms is, however, still constructed using alternating current (AC) [7]. Questions of interest are what types of collection grid topologies can be considered, and limits on AC and direct current (DC) for transmission of power to the shore.

Regardless of how the energy converters are interconnected in an offshore farm and how the power is transmitted to the shore, an important consideration is how an energy converter is interfaced with the grid. Renewable energy sources are often intermittent in nature, which means they are not controllable. The often non-controllable nature of renewable energy sources will need to be considered in the design of the grid connection system. A power converter is often necessary to enable the grid connection. In solar power applications the power converter is a key component used to transform the DC output from the photovoltaic cells to AC power for the distribution grid [8]. Wind power is often interfaced with the electrical grid via a Back-to-Back (B2B) converter, where the AC power from the generator is first rectified to DC and then inverted back to AC [9]. In this way, the generator side and the grid side of the converter topology are decoupled [10]. For marine current power and wave power a power converter will also need to be considered. In the wave power concept developed by Uppsala University and experimentally evaluated at the Lysekil test site in Sweden, passive rectification with a voltage source converter for the grid connection was used [11]. At the marine current converter test site in Söderfors, Sweden, also developed and operated by Uppsala University, a B2B converter is used for the grid connection [12, 13].

The use of a voltage source converter for the grid connection requires special considerations of how the power is conditioned to fulfil grid code requirements [14]. Among others, an electronic filter will often be required at the grid connection point in order to remove high-frequency harmonics in the power [15]. Many different filter technologies can be found in the literature, such as L-, LC- and LCL-filters [16, 17]. Important issues that need to be considered are the stability of the filter and how the filter interacts with the control algorithm used for the voltage source converter [17]. Higher-order filters, like LC- and LCL-filters, have a resonance peak that needs to be considered in the design of the system and potentially handled using a resonance peak damping strategy [17].

This thesis will focus on three topics associated with electrical systems for grid-connected offshore renewable energy sources. Different collection grids and transmission topologies will be considered. The grid connection of a marine current energy converter will be evaluated with simulations. Filter technologies will be discussed and a novel transfer function for a system consisting of an LC-filter and a power transformer will be presented.

1.2 Aim and outline of the thesis

As has been outlined in Section 1.1, many different aspects need to be considered in the grid connection of renewable energy. In Figure 1.1, a possible general summary of the different steps that need to be considered and investigated in the grid connection of offshore renewable energy is illustrated. The

different steps are of course very broad and other categorizations are possible. The first step is the specific energy source, for example, winds, marine currents or waves. The second step is the power conversion, which includes the conversion of mechanical to electrical energy in the generator and the conversion of the electrical energy to suitable voltage levels for AC transmission or the conversion to DC. After the power conversion, the collection grid for the interconnection of energy converters in an offshore farm needs to be considered. Finally, the transmission of power to the shore, and the grid connection to the external electrical grid, for example, the distribution grid, must be investigated.

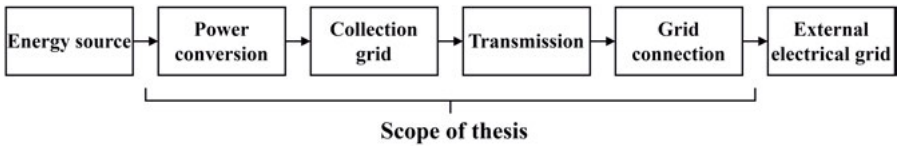

Figure 1.1. Overview of the scope of the thesis.

The aim of this thesis is to investigate electrical systems for grid connection of offshore renewable energy sources. The areas that are more specifically considered are the electrical power conversion of the output from the generator, the collection grid, the power transmission to the shore and the grid connection to the external electrical grid. The design of turbines or buoys, the generator design and the external electrical grid are outside the scope of this thesis.

The objectives of the thesis are:

- To give an overview of AC and DC collection grid topologies and HVAC and HVDC transmission for offshore renewable energy.
- To present a model and simulations of a grid-connected marine current energy converter.
- To give an overview of filter technologies for grid-connected voltage source converters.
- To present a derived transfer function for an LC-filter connected to a power transformer and the verification of the transfer function with simulations and experiments.

The outline of the thesis is the following. In Chapter 2, the thesis begins from the system perspective, where collection grid topologies and HVDC and HVAC transmission are discussed. This chapter is mainly adapted from **Paper II**. Then, a grid connection technology for a marine current energy converter is discussed in more detail in Chapter 3. This part is mainly based on **Paper I**. Filters are reviewed, and a transfer function for an LC-filter connected to a power transformer is derived in Chapter 4. In Chapter 5, the experimental verification of the derived transfer function is presented. These chapters are based on **Paper III**. In Chapter 6, the thesis is summarized and

the most important conclusions are presented, and in Chapter 7 future work is discussed. In Chapter 8, summaries of the papers on which the thesis is based can be found, and finally, in Chapter 9, a summary of the thesis is given in Swedish.

1.3 Marine current power

In this thesis, marine current energy will primarily be considered when offshore renewable energy is discussed. The considered technology is the vertical axis marine current turbine developed by the Division of Electricity at Uppsala University, illustrated in Figure 1.2. The turbine was deployed in the river Dalälven in Söderfors, Sweden, in 2013 [18]. The turbine is five-bladed and constructed to be placed on the riverbed. The generator is mounted on the same axis as the turbine without a gearbox and is of the type permanent magnet synchronous generator (PMSG). The electrical system at the test site is further discussed in Chapter 3.

Marine current power and the development of the turbine and the electrical system at the test site have been the subject of multiple studies. The studies presented in [19, 20, 21] investigate generators for marine current energy conversion. The development of the electrical system at the Söderfors test site is described in [22, 23] and hydrodynamic simulations of the turbine are performed in [24]. The electrical system and the performance of the turbine are experimentally investigated in [25]. Marine current resources are evaluated in [26, 27]. Different research topics in the area of marine current energy conversion are presented in [28].

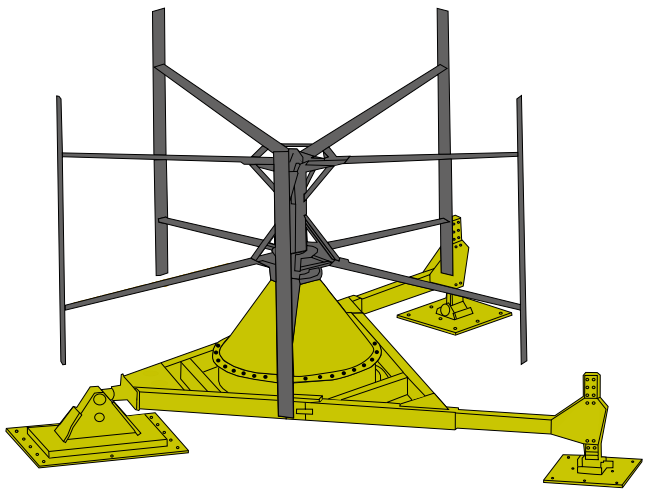

Figure 1.2. The marine current energy converter developed by Uppsala University. Illustration by Anders Nilsson.

2. Grid topologies and power transmission for offshore applications

The electricity generated by offshore renewable energy sources needs to be transmitted to the shore. If multiple energy converters are considered it is suitable to interconnect the energy converters with an offshore collection grid. The dominating grid technology in offshore wind power is AC collection grids [7, 9]. However, as larger wind farms located further from the shore have been commissioned it has been necessary to use HVDC for the transmission of power to the shore. An interesting question here is how a system completely based on DC could be constructed. Furthermore, it can be noted that as of today there are no large-scale marine current or wave power farms. Therefore, it is useful to use offshore wind farms as a template when investigating the potential grid topologies for marine energy sources. In view of these aspects, a review of AC and DC collection grid topologies for offshore renewable energy is presented in this chapter. HVDC and HVAC transmission are also discussed and the techno-economic break-even distance is evaluated in a literature review. The material in this chapter is adapted from **Paper II**.

2.1 AC collection grids

Many different collection grid topologies have been proposed for offshore wind farms in the literature [29, 30, 31, 32, 33, 34]. However, four main topologies can be identified: the *radial topology*, the *single-sided ring topology*, the *double-sided ring topology* and the *star topology*. These topologies will be briefly discussed below. In **Paper II**, the potential costs of components like cables and transformers for offshore applications are also investigated.

2.1.1 Radial topology

The most commonly used topology and also the most simple is the radial topology [32]. The radial topology is illustrated in Figure 2.1. The energy converters are connected to a single feeder cable, which is connected to a bus on land. The bus could also be placed at sea, submerged or on a platform. The bus is in turn connected to the distribution grid at the point of common coupling (PCC). Since the energy converters are connected to a single cable there is no redundancy. If a fault occurs on the cable, all the energy converters on

the side of the fault opposite to the bus are disconnected. The main advantages of the radial topology are that the system is easy to control and that less cable is required compared with, for example, the single-sided ring topology [33]. On the other hand, the main disadvantage is the complete lack of redundancy [33]. The redundancy can however be improved if many radially connected energy converters are connected to a single bus as in Figur 2.1.

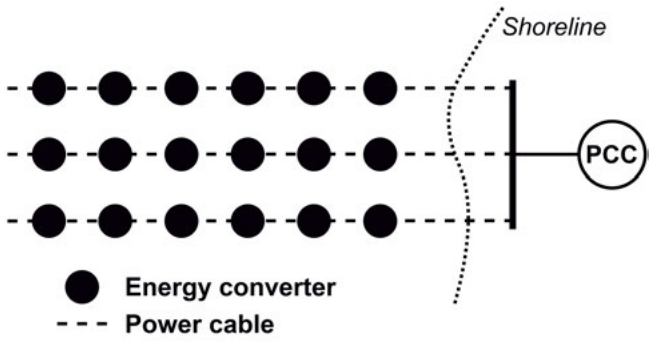

Figure 2.1. Radial topology. The figure is from **Paper II**.

2.1.2 Single-sided ring topology

The lack of redundancy for the radial topology can be mitigated by including a return cable to the shore from the last energy converter in a row, as illustrated in Figure 2.2. This is called a single-sided ring topology. If a fault occurs in the row of energy converters the extra return cable gives the currents an alternative way to reach the bus. The return cable must be rated for the total power of all energy converters connected in a row. The use of a return cable and the need to rate it for the complete farm increases the costs of the single-sided ring topology compared to the radial topology [29].

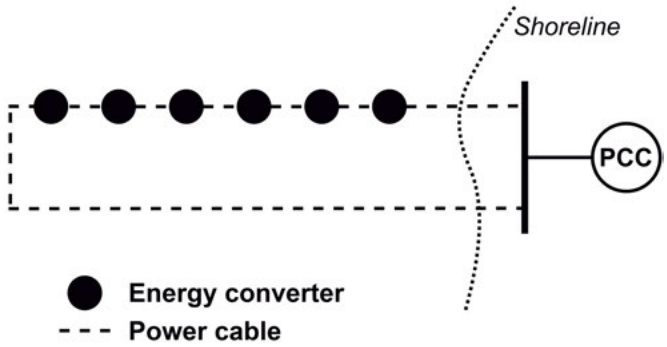

Figure 2.2. Single-sided ring topology. The figure is from **Paper II**.

2.1.3 Double-sided ring topology

The single-sided ring topology can be extended by connecting energy converters to the return cable. This topology is called double-sided ring topology and is illustrated in Figure 2.3. This will reduce the increased cost of having a return cable since the cable will be utilized more effectively. However, if a fault was to occur at either the beginning or the end of the cable, parts of the intact cable need to be able to carry the total power of all energy converters. The cable in the double-sided ring topology will therefore be utilized more effectively but it will be required to have a higher power rating.

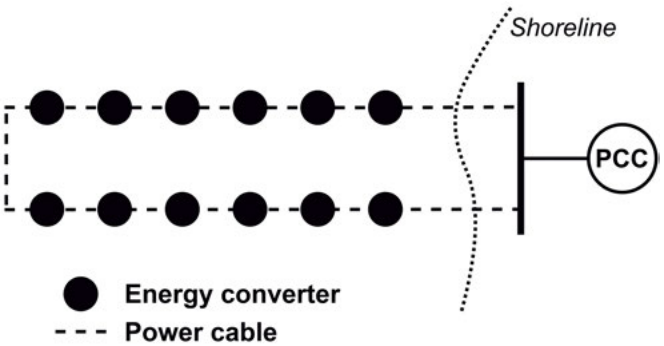

Figure 2.3. Double-sided ring topology. The figure is from **Paper II**.

2.1.4 Star topology

An attempt to reduce the ratings of the cables in the system is the star topology illustrated in Figure 2.4. In the star topology, multiple energy converters are connected to an energy converter located in the center of a star-like configuration. The cable from a single energy converter to the energy converter in the center only needs to be rated for one energy converter. However, the cable to the shore from the energy converter in the center needs to be rated for the total power of all energy converters in the system. Since the energy converters are independently connected to the center unit, the redundancy of the system is good as long as the cable to the shore is intact. The main advantages are the improved security of the system given by the single cables from each respective energy converter and the possibility of these cables to have a lower power rating [29]. The main disadvantage is that more complex switch gear and safety equipment will be required in the energy converter in the center, which might result in significantly increased costs [29].

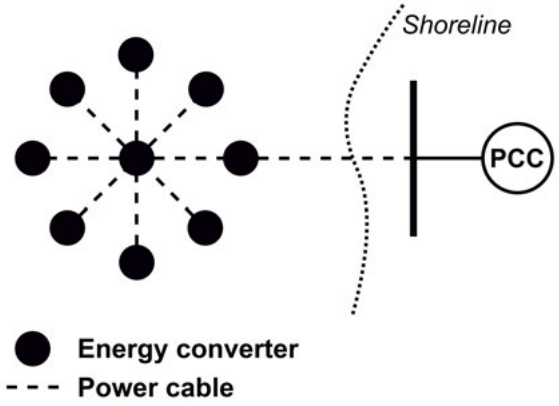

Figure 2.4. Star topology. The figure is from **Paper II**.

2.2 DC collection grids

As previously mentioned, the commercial standard in offshore wind power is AC collection grids. There are no large-scale offshore wind farms that are based on DC collection grids. If the wind farm is large and located far from the shore, the power transmission to the shore is often achieved with HVDC. The internal collection grid in the farm will, however, still be based on AC voltage. HVDC and HVAC transmission are further discussed in Section 2.3. The interest in using DC for collection grids is based on that power losses potentially can be decreased and that DC components can possibly be constructed smaller. The possibility of making components smaller can be especially interesting in marine energy applications, where space limitations can be a very important consideration. This is further explored in **Paper II**.

In the literature two main categories of DC collection grids can be identified: *parallel* and *series* topologies [30, 31, 33, 34, 35, 36]. In the following sections, three parallel topologies and one series-connected topology will be discussed.

2.2.1 Parallel DC collection grids

In the parallel DC collection grid, the energy converters are electrically connected in parallel to the grid. In the ideal case, this means that the voltage over all energy converters is the same. One of the most basic cases of a parallel DC collection grid is illustrated in Figure 2.5. In this case, all energy converters are connected to a single radial feeder cable. The AC voltage from the generator is rectified in each respective energy converter. The DC voltage from the DC collection grid is inverted to AC voltage on land, and the AC power is injected into the distribution grid at the PCC. Concepts for AC to DC voltage

conversion is further discussed in Section 2.2.3, and components for DC/DC and DC/AC conversion are further elaborated in **Paper II**.

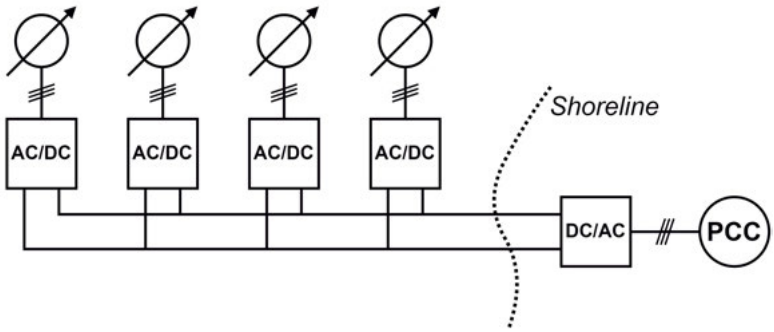

Figure 2.5. Parallel DC collection grid. The figure is from **Paper II**.

The cable from the first energy converter in the row to the onshore DC/AC converter needs to be rated for the total power of all units. The current transmitted to the shore, $i_{dc}(t)$, is given by the following equation:

$$i_{dc}(t) = \sum_{k=1}^{k} i_{do(k)}(t), \tag{2.1}$$

where $i_{do(k)}$ is the current from energy converter k. The number of energy converters that can be connected to one cable will be limited by the power rating of the cable to the shore. Furthermore, since the voltage level is the same over the whole grid, the possible transmission distance to the shore will depend on how much the voltage can be increased in the energy converters. Higher voltage levels will allow for longer transmission distances, see Section 2.3.

It is also possible to consider multiple rows of energy converters connected to an offshore connection point, as shown in Figure 2.6. The connection point is in this case considered a passive component with a busbar and necessary monitoring, control and safety equipment. It can either be submerged, placed above the surface on a seabed-mounted structure or floating. The inclusion of a collection point which is fed with power from multiple parallel rows of energy converters gives the system more redundancy. If a fault occurs on the cable in one row, the other rows can still keep supplying power to the PCC on land. However, would a fault occur on the cable from the connection point to the onshore PCC the complete farm would be disconnected from the distribution grid. The cable to the shore needs to be rated for the power level of the complete farm, while the cable in a row only needs to be rated for the power level in that row. This can be beneficial if large farms are considered. In this case, cables with lower power ratings can be used in the rows and only one high-power cable is needed for the transmission from the collection point to the shore. The possible transmission distance will also here be limited by

the voltage level of the grid and by the capability of the energy converters to increase the voltage. The current in the cable from the connection point to the onshore inverter, $i_{DC}(t)$, can be expressed by the following equation:

$$i_{DC}(t) = \sum_{n=1}^{n} i_{dc(n)}(t), \tag{2.2}$$

where $i_{dc(n)}$ is the current from row n.

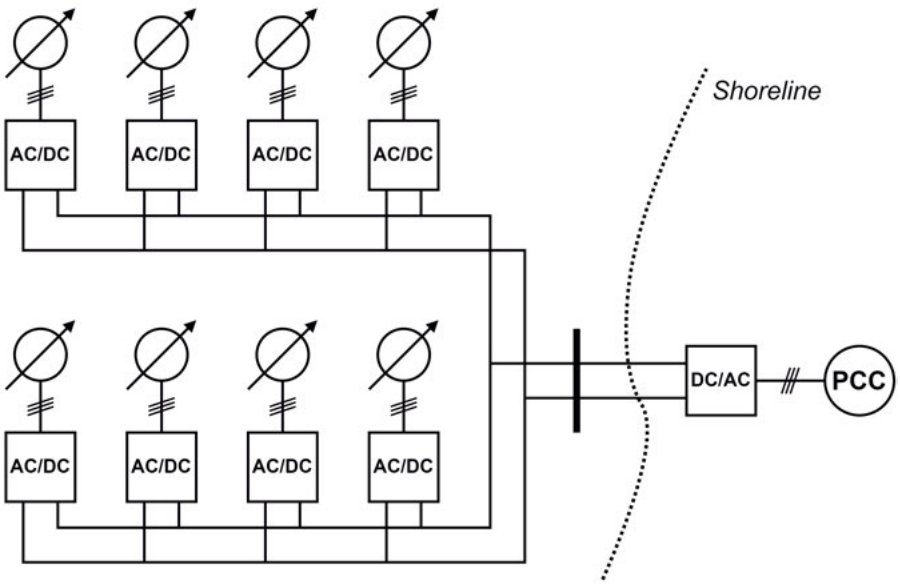

Figure 2.6. Parallel DC collection grid with an offshore connection point. The figure is from **Paper II**.

Since the transmission distances of the discussed topologies are limited by how much the voltage level can be increased in the energy converters, a natural extension is to include a separate voltage boosting stage in the topology, as illustrated in Figure 2.7. This is in essence the same topology as the parallel DC collection grid with an offshore connection point but instead of the passive connection point, an active offshore hub is utilized. The meaning of ”active” is that the component has a more distinct function, which in this case is to increase the DC voltage from the DC collection grid to a higher voltage for the power transmission to the shore. The benefits of the inclusion of a DC/DC converter are that equipment and cable with lower voltage ratings can be used in the offshore grid while HVDC transmission of power to the shore still can be achieved, thus enabling transmission of power over long distances and from large farms. In large wind farms, HVDC transmission is already in use but then the conversion in the offshore hub is from AC to HVDC [7]. The experience from these types of projects is that the offshore platform for AC

to HVDC conversion usually is one of the single most expensive components in the system [37, 38]. Therefore, the DC/DC converter can be expected to be a very expensive component. Also, the complexity of the system is expected to increase since the DC/DC converter will be based on complex power electronic converter systems. DC/DC conversion technologies are further discussed in **Paper II**.

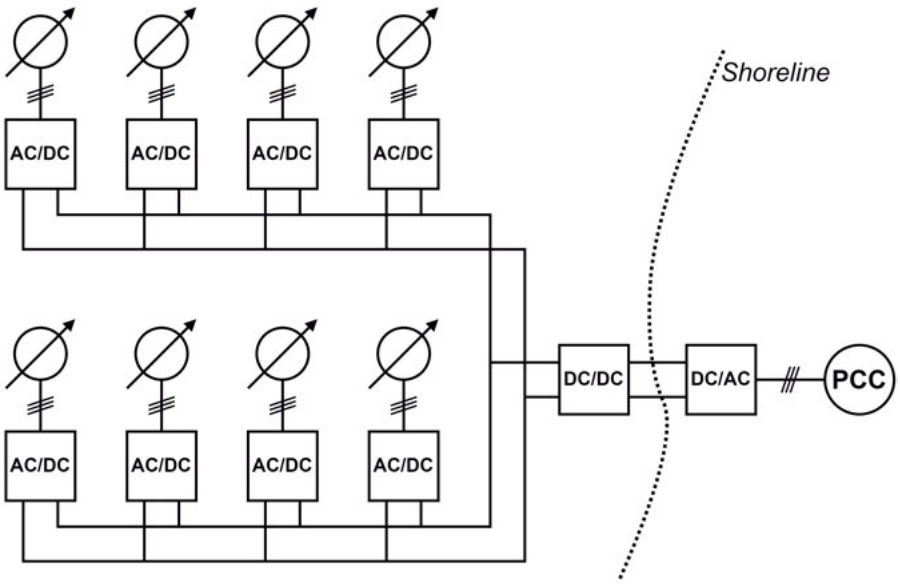

Figure 2.7. Parallel DC collection grid with an offshore hub. The figure is from **Paper II**.

2.2.2 Series DC collection grids

The energy converters can also be connected in series as illustrated in Figure 2.8. Series-connected wind turbines have been explored in [35], where the concept was compared with the AC collection and transmission at the Horns Rev offshore wind farm in Denmark. It was shown that series-connected wind turbines could have lower energy production costs compared to AC topologies. However, because each respective energy converter needs to be able to maintain the output voltage at a certain level and handle large power fluctuations, the energy converters need to be rated 35 % higher than the nominal voltage. Series-connected wind farms have also been considered in [39, 40, 41], where specifically a design with a PMSG, an AC/AC converter, a high-frequency transformer and a passive rectifier was investigated.

The main advantage of series-connected energy converters is that a high voltage level for transmission can be achieved without a separate DC/DC conversion stage either in the energy converter or externally, as in the topology

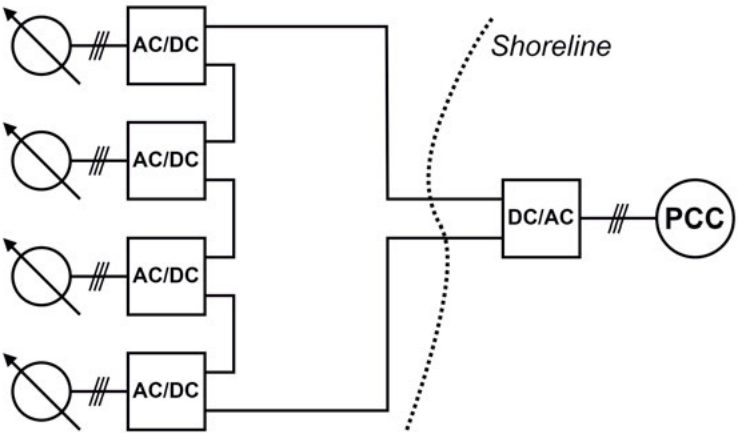

Figure 2.8. Series DC collection grid. The figure is from **Paper II**.

discussed for the parallel DC collection grid with an offshore hub. The transmission voltage, $v_{DC}(t)$, is the sum of the voltages from all energy converters connected in series, as shown in the following equation:

$$v_{DC}(t) = \sum_{k=1}^{k} v_{do(k)}(t), \tag{2.3}$$

where $v_{do(k)}(t)$ is the output voltage from energy converter k.

As has already been implied, the main issue with the series DC topology is that the output voltage from the energy converter needs to be maintained at a specific level in order to keep the transmission voltage at the desired level. Another issue is that the last energy converter in a row of series-connected energy converters may need to be electrically insulated for the full transmission voltage, depending on how the system is electrically grounded. This can make the construction of the electrical insulation expensive and possibly unmanageable.

2.2.3 AC to DC voltage conversion

The DC topologies discussed above require a DC output voltage from the energy converter. Usually, an AC generator is used and therefore an AC to DC conversion step is necessary. Different concepts for how to achieve a DC voltage output from an energy converter are discussed in [42]. Four of these strategies are shown in Figure 2.9. It should be noted that these are only general concepts. How the different components are specifically constructed is a more detailed question.

The most simple approach is to only have a single rectifier, as shown in Figure 2.9(a). The rectifier could either be based on an active or a passive technology. The output voltage will, however, be limited by the nominal ter-

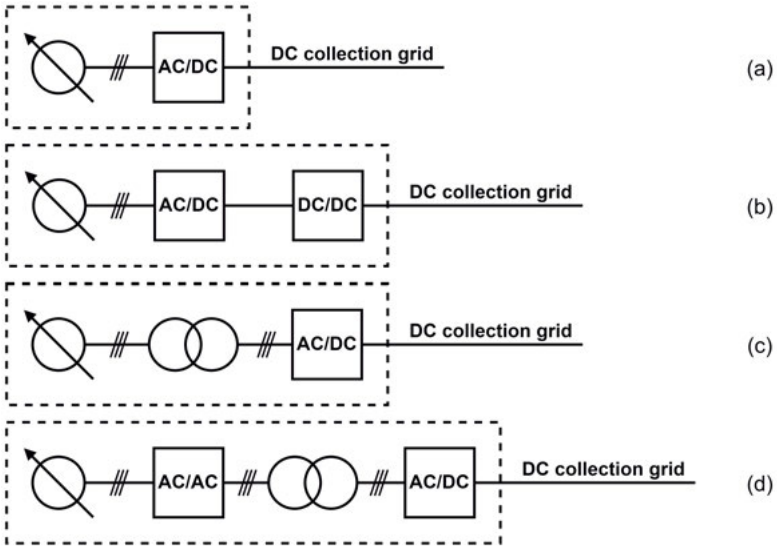

Figure 2.9. Concepts for AC to DC conversion in energy converters using: (a) only a rectifier; (b) a rectifier and a DC/DC converter to increase the voltage; (c) a low-frequency transformer to increase the voltage and a rectifier; (d) an AC/AC converter to increase the frequency of the voltage, a high-frequency transformer to increase the voltage level and a rectifier. The figure is from **Paper II**.

minal voltage of the generator [42]. Another issue with this topology is the lack of galvanic isolation between the generator and the grid.

In Figure 2.9(b), a concept with two stages is shown. First, the AC output from the generator is rectified with either a passive or an active rectifier. The DC voltage is then increased with a DC/DC converter. An advantage of this concept is that the voltage can be increased to higher levels. Furthermore, it is possible to construct a DC/DC converter with galvanic isolation, which improves the safety of the system. It can be observed that this concept is very similar to a B2B converter, which is further explored in Chapter 3.

Another approach that also utilizes two separate stages is shown in Figure 2.9(c). Here an ordinary low-frequency transformer is placed directly after the generator. The transformer is used to increase the voltage and galvanically isolate the generator from the grid. The increased voltage is then rectified with either a passive or an active rectifier. The main advantage of this topology is its simplicity. Low-frequency transformers are an established technology and are fairly easy to construct. However, transformers are usually very heavy and bulky, which creates difficulties in offshore applications, especially in marine energy, where space is often a limiting factor.

In Figure 2.9(d), a concept that utilizes a high-frequency transformer is shown, which is the concept explored in [39, 40, 41]. An AC/AC converter is used to increase the frequency of the generator voltage. The high-frequency

transformer is then used to increase the voltage, which afterwards is rectified. The mass of a transformer is inversely proportional to the frequency. This means that when the frequency is increased the transformer can be made smaller in size. Therefore, the major advantages of this concept are that an increased voltage and galvanic isolation can be achieved with smaller and lighter components. However, the complexity of the system is increased with the inclusion of the AC/AC converter.

2.3 HVAC and HVDC transmission in offshore applications

For transmission of power over long distances it is often necessary to use HVAC or HVDC in order to avoid high power losses. Traditionally, offshore wind farms have used HVAC. However, as the trend has been towards large wind farms located far from the shore, HVDC transmission has attracted more attention [7, 43, 44]. Two reasons why HVAC has been considered are that conventional transformers can be used to adjust the voltage levels and that the protection system is easier to design compared to HVDC [44]. Furthermore, the HVAC technology has also been in use for a long time and can therefore be considered a more mature technology.

The capacitance of HVAC cables is high, which can give rise to resonance issues and reduce the power that can be transmitted due to the high charging current. The charging current can be reduced by installing reactive power compensation units [45]. The compensation should preferably be installed at several points along a transmission cable. However, due to technical limitations, it is often only possible to install compensation units at the receiving and the sending end of a cable, which results in a limited compensation of the system [45]. HVDC, on the other hand, has no, or very low charging current. This reduces the losses and the voltage drop across the cable, which also increases the amount of power that can be transmitted compared with HVAC.

An HVDC system does, however, require more complex power electronic components compared with traditional HVAC systems. Converter stations for AC/DC and DC/AC conversion are very expensive, which means that HVDC systems usually have a significantly higher fixed cost compared to HVAC [46]. However, since HVDC requires less cable material and exhibits lower power losses, the marginal cost per km is expected to be less for HVDC compared to HVAC. The choice of technology is often decided by the break-even point where HVDC becomes the less expensive option. In a first stage, the break-even point is often evaluated with a techno-economical analysis with regard to factors like the transmission distance and the size of the farm. However, the final decision for a specific offshore renewable energy project will also depend on site-specific conditions, for example, the terrain and local regulations [46].

The break-even point between HVAC and HVDC has been evaluated in multiple studies. In [47], a break-even distance of 50 km to 80 km is expected, while in [48], a distance of 30 km to 50 km is suggested, depending on the HVDC technology, size of the farm and the details of the project. In [49], a study on a 100 MW wind farm suggested a break-even distance of 90 km and in [50], the break-even distance was estimated to be 120 km to 160 km for a 1 GW wind farm. Break-even distances from these two studies and from [45, 51, 52, 53, 54, 55] are compiled in Figure 2.10. It should be observed that in [51] multiple distances are reported, depending on the size of the farm. Therefore, a size of 1200 MW is selected for which the break-even distance is in the range of approximately 135 km to 180 km. The midpoint of which at 157 km is reported in Figure 2.10. Similarly, multiple distances are reported in [52], depending on the power level. Therefore, a farm size of 1200 MW is selected here as well. The vertical axis of the figure shows the power level of the considered wind farm and the horizontal axis shows the proposed break-even distance. As can be observed from the figure, the spread of possible break-even distances is very wide. Furthermore, as previously mentioned, the break-even distance will also be affacted by the size of the farm. However, for transmission distances above 50 km to 100 km the studies appear to indicate that the preferred transmission technology is HVDC. This range is also concluded in a review in [46].

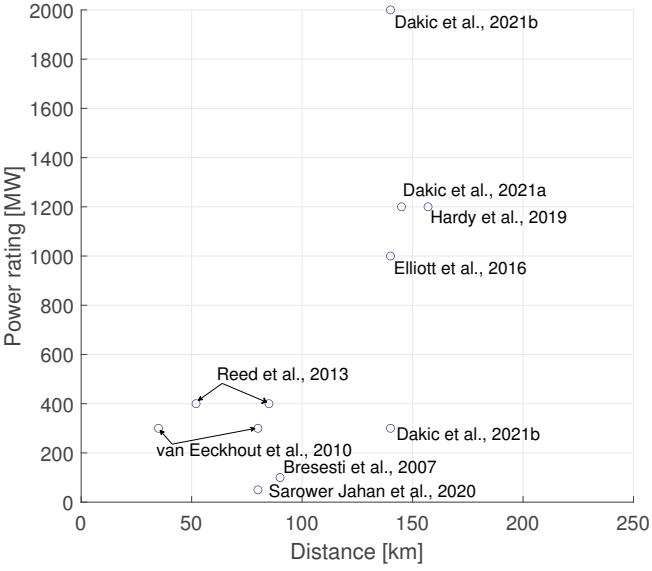

Figure 2.10. Break-even distances reported in studies [45, 49, 50, 51, 52, 53, 54, 55]. Dakic et al. 2021a refers to [52] and Dakic et al. 2021b refers to [55]. Studies appearing twice have analyzed multiple scenarios. The figure is from **Paper II**.

3. Grid-connected renewable energy sources

An important question for renewable energy is how the energy converter is connected to the electrical grid. This grid can be a farm internal grid as discussed in Chapter 2 or the external distribution grid. A grid connection system often requires a power converter and a filter to achieve a voltage and current suitable for the grid. In this chapter, the grid connection of a marine current energy converter connected to an AC distribution grid is considered. The focus of this chapter is on the electrical control system. A simulation model of the system is presented. The material in this chapter is mainly based on **Paper I**.

3.1 General considerations for grid connection

Renewable energy sources are often characterized by varying power generation. For grid code compliance, a stable and sinusoidal voltage at 50 Hz or 60 Hz is required. More specifically, in order to connect to the distribution grid the following fundamental criteria need to be fulfilled:

- The voltages must be in phase with the voltages of the grid, that is, the difference in phase angle must be close to zero.
- The frequency must be the same as the frequency of the grid.
- The amplitudes of the voltages must be the same as the amplitudes of the grid voltages.
- The phase sequence must be the same as the phase sequence of the grid.

Furthermore, the power quality at the PCC must meet certain standards. There are no international standards detailing the responsibility of the energy supplier [56]. However, local standards exist, for example, EN 50160 for low voltage grids in the European Union [56]. The standard EN 50160 imposes requirements on, among others, frequency variations, voltage variation and total harmonic distortion. The specific grid code requirements for grid connection will be determined by the relevant transmission system operator (TSO) or other regulating authority.

The grid connection system must be able to fulfil the grid code requirements. A system often utilized in wind power that is able to do this is the B2B converter [10]. In the following chapters, a simulation model for such a system implemented on the marine current energy converter from Section 1.3 will be presented.

3.2 A grid-connected marine current energy converter

The electrical energy from a marine current energy converter, wind energy converter or wave energy converter varies due to the nature of the energy source. Ocean currents are more predictable than winds and waves. Still, the resources are not controllable like hydropower, where water can be stored in a dam. Since the electrical grid requires a stable AC voltage and current, it is often not suitable to connect the generator directly to the grid. In order to achieve a voltage and current suitable for the electrical grid, a B2B converter can be used to electrically decouple the generator from the grid [10]. The electrical system for the marine current energy converter at the Söderfors test site is based on a B2B converter technology, as shown in Figure 3.1. Starting from the energy source, the system at the Söderfors test site consists of the following parts. A turbine is used to convert the energy in the moving water to mechanical energy. The mechanical energy from the turbine is converted to electrical energy by the generator, which at the test site is a PMSG. The generator is connected to a 2-level voltage source converter (2L-VSC) through an LC-filter. The LC-filter together with the internal inductance of the generator form an LCL-filter. The 2L-VSC is used to convert the AC voltage and current from the generator to DC voltage and current. The converter on the generator side is connected via a DC-link to a 3-level voltage source converter (3L-VSC), which on the AC side is connected to the distribution grid through an LC-filter and a transformer. The LC-filter together with the inductance of the transformer form an LCL-filter. The main function of the grid side converter is to convert the DC voltage and current on the DC-link to AC voltage and current for the grid connection. The purpose of the transformer is to increase the voltage to the correct level for the distribution grid and galvanically isolate the electrical system, including the generator, from the distribution grid.

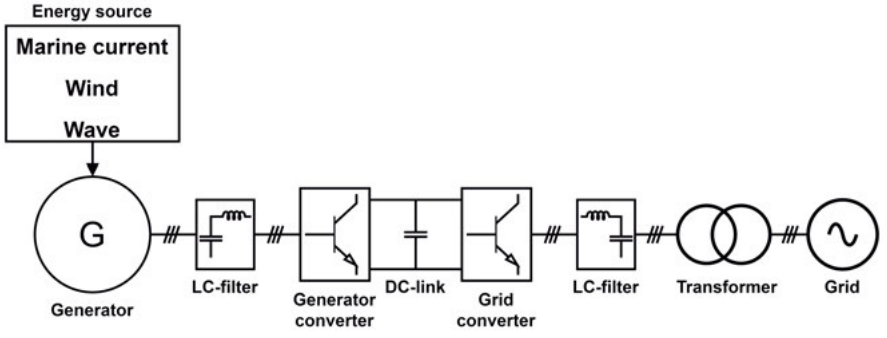

Figure 3.1. A B2B grid connection system. The system implemented at the Söderfors test site. The figure is from **Paper III**.

The system at the test site is bidirectional, which means that the power can be transferred from the generator to the grid and from the grid to the generator.

The turbine is generally not self-starting, and therefore to start up the turbine, it is necessary to use power from the grid to run the generator as a motor in order to achieve a rotational speed high enough for the turbine to start rotating by itself [57]. However, in this chapter, only the direction of power from the generator to the grid will be considered.

A B2B converter requires a control system to function. In the two following sections, a version of the control system implemented at the Söderfors test site is presented. The control system is verified in simulations that are presented in Section 3.3. Since the B2B converter enables the generator side and the grid side of the system to be controlled independently of each other, the control system for the respective part of the system will be discussed separately.

3.2.1 Control of generator side converter

The generator side converter is used to rectify the AC voltage and current from the generator and to control the generator. The implemented control algorithm is field-oriented control (FOC) with zero d-axis current. This control method is supplemented with a maximum power point tracking (MPPT) control scheme to achieve optimal power extraction from the turbine. The generator side control is shown in Figure 3.2.

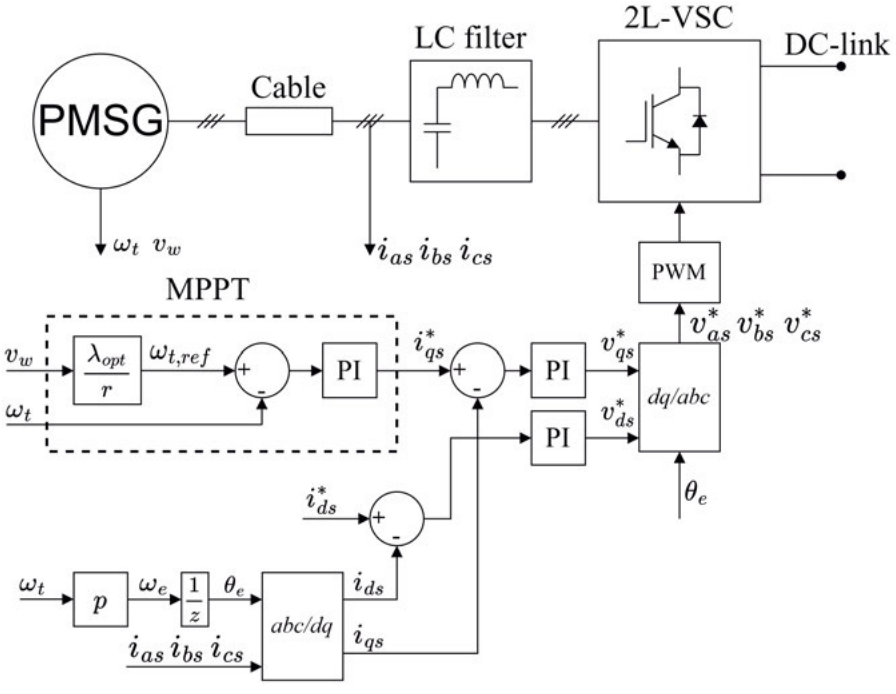

Figure 3.2. The generator side control system for a B2B converter. The figure is from **Paper I**.

In FOC with zero d-axis current, the phase currents i_{as}, i_{bs} and i_{cs} from the generator are first transformed into a rotating coordinate system using a dq-transformation. The generator is then controlled by the dq-axis currents i_{ds} and i_{qs}. The d-axis current is maintained at zero by using a PI controller and reference value $i_{ds}^* = 0$. If $i_{ds} = 0$, the q-axis current, i_{qs}, is equal to the stator current of the generator [10]. Then it is possible to show that the electromagnetic torque of the generator is given by the following equation:

$$T_e = \frac{3}{2} p \psi_r i_{qs}, \tag{3.1}$$

where p is the number of pole pairs and ψ_r is the rotor flux linkage. If the rotor flux linkage is constant, the relationship between the torque and the q-axis current is linear. From Equation 3.1 it can be concluded that by controlling the q-axis current, the electromagnetic torque can be controlled, which in turn will enable control of the angular velocity of the turbine.

The MPPT scheme aims to achieve the optimal tip speed ratio, λ_{opt}, for the turbine by regulating the angular velocity of the turbine. The power captured by the turbine from the moving water is maximized when the tip speed ratio is at its optimal value. Therefore, if the angular velocity of the turbine is adjusted to achieve λ_{opt} for a given water speed, the power from the turbine is maximized. The tip speed ratio is given by:

$$\lambda = \frac{\omega_t r}{v_w}, \tag{3.2}$$

where ω_t is the angular speed of the turbine, r is the radius of the turbine rotor and v_w is the water speed. As can be observed in the MPPT block in Figure 3.2, the input variables to the block are v_w and ω_t. Equation 3.2 is used with λ_{opt} to calculate a reference value for the angular velocity of the turbine, $\omega_{t,ref}$, which is compared with the actual angular velocity of the turbine. The error is sent to a PI controller and the output from the controller is the reference for the q-axis current, i_{qs}^*.

The reference q-axis current is compared with the measured i_{qs} and the error is sent to a PI controller, which generates a q-axis voltage reference, v_{qs}^*. As already observed above, the same is done with the reference d-axis current but this gives the d-axis voltage reference, v_{ds}^*. The dq-axis voltage references are transformed back to a stationary coordinate system and used as reference signals for a pulse-width modulation (PWM) block, which generates control pulses for the 2L-VSC.

3.2.2 Control of grid side converter

The grid side converter is supposed to convert the DC voltage and current from the DC-link to AC voltages and currents that can be injected into the distribution grid. The converter is also supposed to maintain the voltage level

of the DC-link. To achieve this, voltage oriented control (VOC) with a phase locked loop (PLL) scheme is implemented, as illustrated in Figure 3.3.

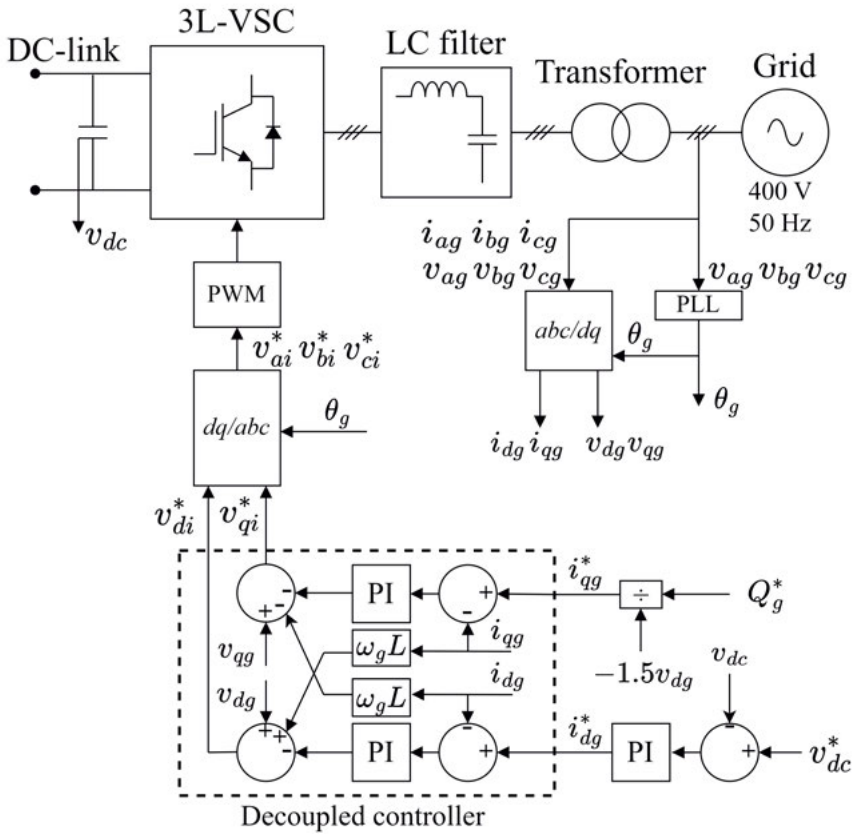

Figure 3.3. The grid side control system for a B2B converter. The figure is adapted from **Paper I**.

The PLL algorithm uses the grid voltages to detect the grid voltage angle, θ_g, which is used for the transformation of the voltages and currents from a stationary to a rotating coordinate system.

The VOC method requires that the d-axis of the rotating coordinate system is aligned with the grid voltage vector. If this is the case, the magnitude of the d-axis component of the grid voltage will be equal to the magnitude of the grid voltage vector [10]. The q-axis voltage will in this case be zero and the active and reactive power exchanged with the grid can be shown to be given by the following equations:

$$P_g = \frac{3}{2}(v_{dg}i_{dg} + v_{qg}i_{qg}) = \frac{3}{2}v_{dg}i_{dg}, \tag{3.3}$$

$$Q_g = \frac{3}{2}(v_{qg}i_{dg} - v_{dg}i_{qg}) = -\frac{3}{2}v_{dg}i_{qg}. \tag{3.4}$$

Equation 3.4 can be rewritten to give an expression for the grid q-axis current, i_{qg}, in terms of the reactive power exchanged with the grid. In the control system in Figure 3.3 this is used to generate a reference current for the controller. If Q_g is set to zero unity power factor operation can be achieved. The grid q-axis reference current from Equation 3.4 is given by:

$$i_{qg}^{*} = \frac{Q_g^{*}}{-1.5 v_{dg}}. \tag{3.5}$$

As already observed, the LC-filter together with the transformer constitutes an LCL-filter. However, it is customary to disregard the filter capacitor when designing a controller for a grid-connected voltage source converter with an LCL-filter. If a voltage source converter with an L-filter is considered, it can be shown that the state equations for the AC side of the converter are given by the following system of equations [10]:

$$\begin{aligned} L\frac{di_{dg}}{dt} &= \left(v_{dg} - v_{di} + \omega_g L i_{qg}\right) \\ L\frac{di_{qg}}{dt} &= \left(v_{qg} - v_{qi} - \omega_g L i_{dg}\right) \end{aligned} \tag{3.6}$$

where v_{di} and v_{qi} are the dq-voltages of the converter phase voltages and ω_g is the angular frequency of the grid. As can be observed in Equation 3.6, the d- and q-axis components are coupled by the terms $\omega_g L i_{qg}$ and $\omega_g L i_{dg}$. It is possible to implement a decoupled controller, which is shown in the block "Decoupled controller" in Figure 3.3. By doing this, the control of the d-axis current is only dependent on d-axis components, and the q-axis current is solely dependent on q-axis components. The design of PI controllers is much simplified and it becomes much easier to achieve a stable system by using a decoupled controller [10].

The DC-link voltage level is maintained by controlling the grid d-axis current. As shown in Figure 3.3, the measured voltage level on the DC-link, v_{dc}, is compared with a reference value, v_{dc}^{*}. The error is sent to a PI controller, which generates a reference value for the grid side d-axis current, i_{dg}^{*}.

The decoupled controller generates reference voltages v_{di}^{*} and v_{qi}^{*} for the control of the 3L-VSC. The dq-voltages are transformed to phase voltages using a dq to abc transformation. The phase voltages are then used as reference signals in the PWM block to generate control pulses for the converter.

3.3 Simulation model

The model presented in Sections 3.2.1 and 3.2.2 was in the study in **Paper I** implemented in MATLAB/Simulink. The model was implemented using built-in blocks and functions from the Simulink software. The parameters used

in the simulation model and more details about the simulations can be found in **Paper I**.

The model was evaluated for three cases: 1) steady-state simulations, 2) simulations with step changes in water speed, and 3) simulations with real water speed data from the Söderfors test site. The simulation model was also used to evaluate the power losses of the system. In the following section, results from the simulations with real water speed data will be discussed. The other parts can be found in **Paper I**.

3.3.1 Simulation results

In Figure 3.4 the performance of the generator side controller is evaluated. The red curve is the water speed and the blue curve is the angular velocity of the turbine. The yellow curve shows the tip speed ratio normalized with regards to the optimal value for the turbine, 3.05. As the water speed is changed, the controller is able to adjust the angular velocity of the turbine. The normalized tip speed ratio is maintained at one indicating that the FOC with the MPPT algorithm is able to achieve a maximized power extraction from the turbine.

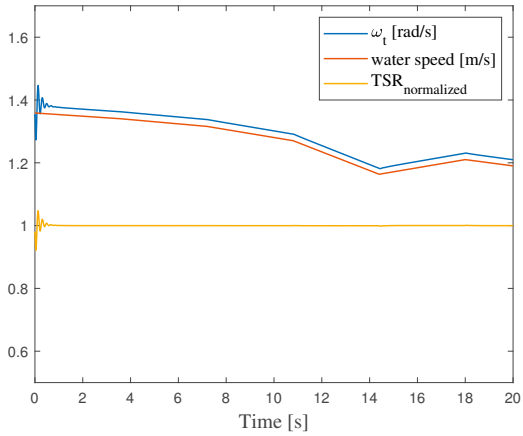

Figure 3.4. Turbine angular velocity, water speed and tip speed ratio (TSR) for the turbine normalized around the optimum at 3.05 during a simulation using measured water speeds as input to the turbine. The figure is from **Paper I**.

The grid side converter is supposed to inject the power from the turbine into the grid. In Figure 3.5, the power injected into the grid is shown together with the power from the turbine. As can be seen, the power injected into the grid changes with changes to the water speed. When the water speed decreases the power from the turbine decreases, which also means that less power is injected into the grid. The opposite occurs when the water speed is increased.

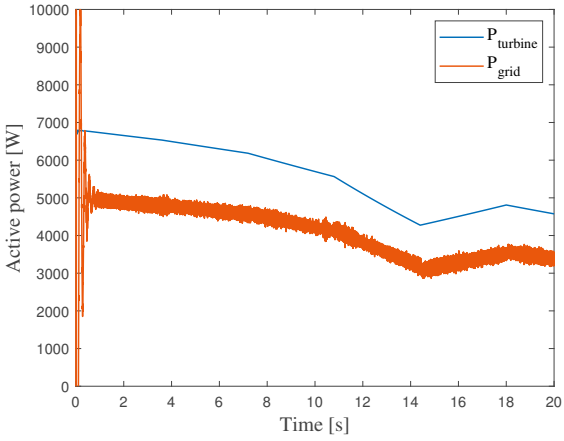

Figure 3.5. Mechanical power injected into the generator and electrical power injected into the grid during a simulation using measured water speeds as input to the turbine. The figure is from **Paper I**.

Finally, Figure 3.6 shows the DC-link voltage. The reference value is 400 V. When the simulation starts there are some initial transients. However, within 2 s the DC-link voltage is stabilized around the reference value and the VOC is able to maintain this value even when the water speed changes. The measured DC voltage is never more than 0.05 % from the reference value.

Since the grid side converter is able to inject power into the grid while maintaining the DC-link voltage, the grid side controller works as expected.

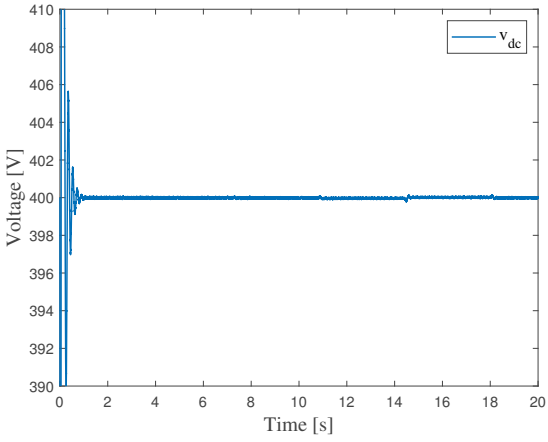

Figure 3.6. The voltage on the DC-link during a simulation using measured water speeds as input to the turbine. The figure is from **Paper I**.

4. Filters and transformers

In Chapter 3 it was observed that two important parts of a grid connection system are filters and transformers. The filter is used to remove high-order harmonics from AC voltages and currents. A 2L-VSC or a 3L-VSC will not create perfect sinusoidal voltages and currents, and therefore a filter will be necessary for the grid connection to fulfil grid code requirements. A transformer is used to regulate the voltage to a desired level. Therefore, a transformer will often be required to adjust the voltage from the voltage source converter to a suitable level for the grid. Furthermore, a transformer makes the electrical system galvanically isolated from the grid, which from a safety perspective is advantageous. In this chapter L-, LC- and LCL-filters will be discussed. A common model for a non-ideal power transformer will also be presented. Finally, a model for an LC-filter connected to a power transformer will be introduced, and a transfer function will be derived for the model. The material in this chapter is adapted from **Paper III**.

4.1 L-, LC- and LCL-filters

One of the main purposes of filters in the context of grid-connected voltage source converters is to ensure that grid code requirements are followed by removing high-frequency harmonics, which are usually created by the PWM control of the voltage source converter [16, 58]. The three common filter technologies L-, LC- and LCL-filter are shown in Figure 4.1. The damping capability and behaviour of filters are usually analysed in the frequency domain. In this section, the basic circuits for the three filter technologies will be presented. The transfer functions for the circuits will be given and the frequency response of the filters will be evaluated.

One of the most basic filter technologies is the L-filter, which is shown in Figure 4.1(a). The L-filter consists of one single inductor, L, with the impedance $Z_L = sL$ in the Laplace domain. To fulfil grid code requirements a large inductance value is usually required. This makes the filter bulky and will result in a large voltage droop over the component [58]. The filter will also have a slow time response [58]. Because of these factors, the L-filter is usually not considered a feasible option for grid-connected voltage source converters.

The frequency response of the L-filter is usually analysed with the transfer function from the input voltage, V_{in}, to the output current, I_{out}. The input voltage is here the AC voltage from the voltage source converter and the output

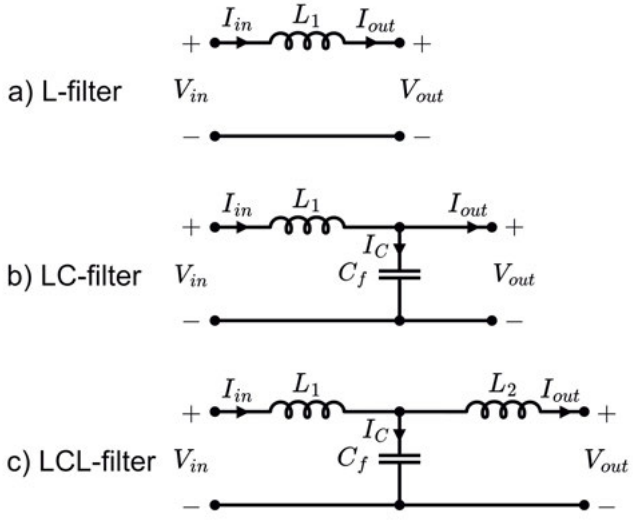

Figure 4.1. Single-phase equivalent circuits for a) L-filter, b) LC-filter and c) LCL-filter. The figure is from **Paper III**.

current is the current injected into the grid. The transfer function for the L-filter is given by the following expression:

$$H_L = \frac{I_{out}}{V_{in}} = \frac{1}{sL_1}. \tag{4.1}$$

The Bode plot for the transfer function in Equation 4.1 with a generic inductance value is shown in Figure 4.2. As can be observed in the figure, the L-filter has an attenuation rate of $-20\,\mathrm{dB/dec}$.

A natural extension of the L-filter is to create a low-impedance path for high-frequency harmonics by including a shunt-connected capacitor, C. The circuit for an LC-filter is shown in Figure 4.1(b). The frequency response of the LC-filter is usually analysed with the transfer function from the input voltage, V_{in}, to the output voltage, V_{out}. The output voltage corresponds to the grid voltage. The transfer function for an LC-filter is given by:

$$H_{LC} = \frac{V_{out}}{V_{in}} = \frac{1}{L_1 C_f s^2 + 1}, \tag{4.2}$$

and as can be observed it is a second-order filter. The frequency response of the LC-filter is shown in Figure 4.2. The high-frequency attenuation rate for LC-filters is $-40\,\mathrm{dB/dec}$. Furthermore, as can be observed in Figure 4.2, the frequency response of the LC-filter is characterised by a distinct resonance frequency. It can be shown that the resonance frequency is given by the following

equation:

$$\omega_{res,LC} = \frac{1}{\sqrt{L_1 C_f}}. \tag{4.3}$$

If a second inductor is included a third order LCL-filter is formed. The circuit for an LCL-filter is shown in Figure 4.1(c) and it can be shown that the transfer function for an LCL-filter is given by the following equation:

$$H_{LCL} = \frac{I_{out}}{V_{in}} = \frac{1}{L_1 L_2 C_f s^3 + (L_1 + L_2)s}. \tag{4.4}$$

As can be observed in the Bode plot for the LCL-filter in Figure 4.2, the LCL-filter, similarly to the LC-filter, exhibits a resonance peak at a certain frequency. This frequency can be shown to be given by the following equation:

$$\omega_{res,LCL} = \sqrt{\frac{L_1 + L_2}{L_1 L_2 C_f}}. \tag{4.5}$$

The high-frequency attenuation rate of the LCL-filter is $-60\,\mathrm{dB/dec}$, which is substantially higher than the attenuation rate of the L- and LC-filter. A significant advantage of the LCL-filter is that smaller capacitance and inductance values can be used compared with the L- and LC-filter, while the LCL-filter still have a superior high-frequency attenuation rate [16].

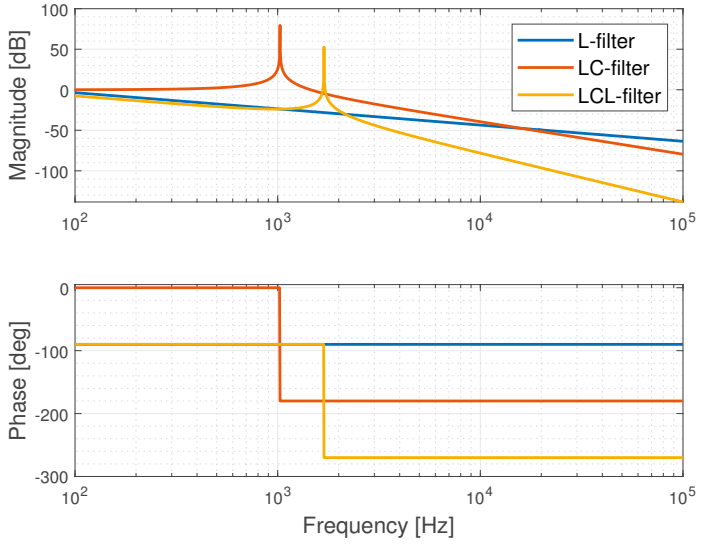

Figure 4.2. Bode plot for L-, LC- and LCL-filter transfer functions for a generic selection of filter parameters. The figure is from **Paper III**.

4.1.1 Resonance peak damping techniques

The occurrence of a resonance peak in the frequency response of the LC- and LCL-filter can create issues with regard to the control of voltage source converters [17]. Therefore, it can be necessary to decrease or completely remove the resonance peak. Broadly, there are two damping techniques: passive damping and active damping. Passive damping is based on the inclusion of passive circuit elements like resistors, inductors or capacitors in the circuit to dampen the resonance peak [17, 59]. A simple and efficient way to dampen the resonance peak of an LCL-filter using passive damping is to series-connect a resistor with the filter capacitor [17].

In active damping techniques, the control structure of the system is modified to achieve a virtual damping of the resonance peak [17, 59, 60]. The active damping techniques can be divided into techniques that do or do not require additional sensors [60].

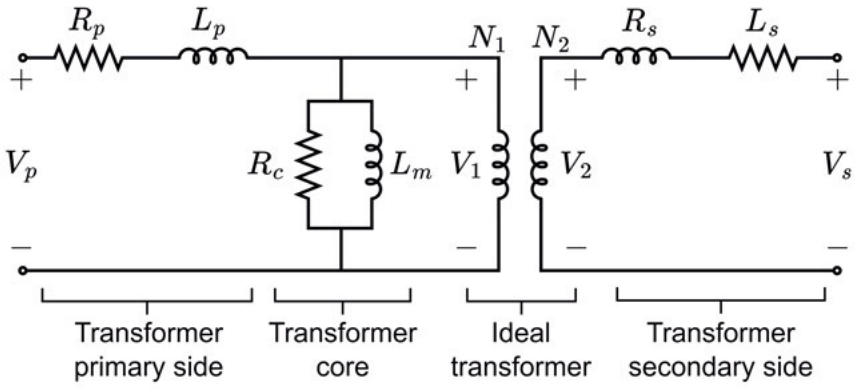

Figure 4.3. Single-phase non-ideal transformer equivalent circuit model. The figure is from **Paper III**.

4.2 Power transformers

The main purpose of a transformer is to adjust the voltage to a desired level. For a grid-connected voltage source converter, this mainly means adjusting the voltage from the converter to a suitable level for the PCC. An additional benefit of using a transformer is that the electrical system of the energy converter is galvanically isolated from the electrical grid.

A common model for a non-ideal transformer is shown in Figure 4.3. The model consists of the following parts:

- An ideal transformer with turns ratio $n = N_1/N_2 = V_1/V_2 = I_2/I_1$, where N_1 and N_2 are the numbers of turns in the primary and secondary windings, respectively. V_1 and I_1 are the voltage and current on the primary

side of the transformer, respectively. V_2 and I_2 are the corresponding quantities for the secondary side of the transformer.

- The primary and secondary side leakage inductance, L_p and L_s. Ideally, all the flux is contained in the iron core of the transformer. However, in a non-ideal transformer some flux is created in the surrounding air of the transformer, which in the model is represented by the leakage flux inductances.
- The primary and secondary side copper resistance of the windings, R_p and R_s.
- The core losses, R_c, which incorporate the losses due to hysteresis and eddy currents in the core.
- The magnetizing inductance, L_m, which models the magnetization of the core material.

4.3 LC-filter and power transformer

As has already been discussed, the electrical system at the Söderfors test site includes an LC-filter and a power transformer at the connection point to the distribution grid. In order to evaluate the frequency response of the system, the derivation of a transfer function for an LC-filter connected to a non-ideal power transformer is presented in this section. The goal is to achieve an expression similar to the transfer function for the LCL-filter in Equation 4.4. In Chapter 5, the verification process of the derived transfer function based on simulations and an experimental study is presented.

The proposed model is shown in *circuit 1* in Figure 4.4 and consists of an LC-filter and a non-ideal transformer. The AC voltage from the voltage source converter is represented by a sinusoidal voltage source. The inductance of the filter is represented by L_f and the resistance of the filter is R_f. The capacitance of the filter is given by C_f. The resistance of a capacitor is usually very small and can therefore be disregarded [61]. The LC-filter is connected to the secondary side components of the transformer, namely the winding resistance, R_s, and the leakage flux, L_s. The primary side of the transformer is connected to the grid. The grid is short-circuited for the purpose of deriving the system transfer function. The elements of the primary side of the transformer are the primary side winding resistance, R_p, and the primary side leakage inductance, L_p. The core resistance, R_c, and magnetising inductance, L_m, are also on the primary side of the transformer.

In order to derive a transfer function from the input voltage to the grid current for the system, $H_{LCT} = I_g/V_{in}$, the circuit is simplified in two steps. First, the components on the primary side are referred to the secondary side of the transformer, which gives *Circuit 2* in Figure 4.4. The series components of the primary side referred to the secondary side are given by $Z'_p = Z_p/n^2$,

where $Z_p = R_p + sL_p$. The core components referred to the secondary side are given by $Z'_{R_c} = Z_{R_c}/n^2$ and $Z'_{L_m} = Z_{L_m}/n^2$, where $Z_{R_c} = R_C$ and $Z_{L_m} = sL_m$.

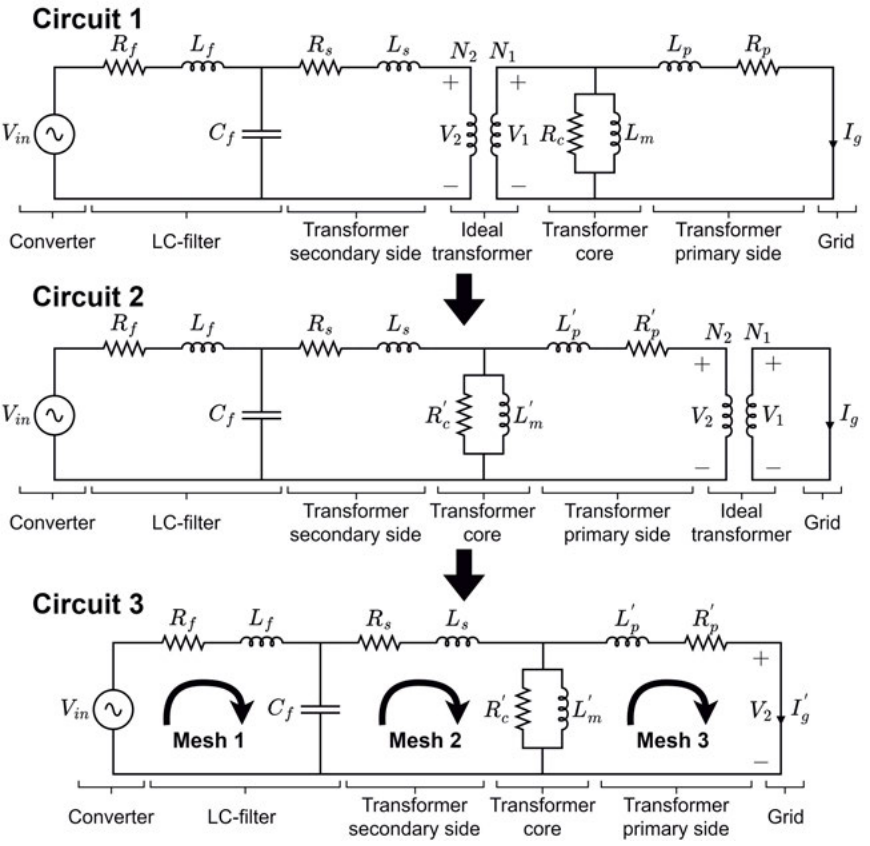

Figure 4.4. Steps in the simplification of the circuit model for the derivation of a system transfer function. Circuit 1: LC-filter and non-ideal transformer. Circuit 2: LC-filter and non-ideal transformer with all parts of the transformer referred to the secondary side of the transformer. Circuit 3: The final simplified LC-filter and non-ideal transformer circuit, where the mesh towards the grid is disregarded since $V_1 = 0$. The figure is adapted from **Paper III**.

Since the primary side of the transformer is short-circuited it can be observed that $V_1 = 0$, which means that $V_2 = V_1/n = 0$. Therefore, the circuit can be simplified further by removing the mesh on the primary side of the transformer. By removing this mesh, the circuit is simplified to *Circuit 3* in Figure 4.4. The grid current expressed on the secondary side of the ideal transformer is given by $I'_g = I_g \cdot n$. Circuit 3 now consists of three meshes and by using standard mesh analysis with $I'_g = I_g \cdot n$ and linear algebra it can be shown that the transfer function for the system is given by the following equation:

$$H_{LCT} = \frac{I_g}{V_{in}} = \frac{1}{n} \cdot \frac{s^1 a_1}{s^5 b_5 + s^4 b_4 + s^3 b_3 + s^2 b_2 + s^1 b_1 + s^0 b_0}. \tag{4.6}$$

The coefficients in the numerator and the denominator are given by the following equations:

$$a_1 = R'_c L'_m, \tag{4.7}$$

$$b_0 = R'_c (R_f R'_p + R_s R'_p), \tag{4.8}$$

$$\begin{aligned} b_1 =& L'_m (R_f R'_p + R_s R'_p) \\ &+ R'_c (R_f L'_p + L_f R'_p + C_f R_f R_s R'_p + R_s L'_p + L_s R'_p) \\ &+ L'_m R'_c (R_f + R_s + R'_p), \end{aligned} \tag{4.9}$$

$$\begin{aligned} b_2 =& L'_m (R_f L'_p + L_f R'_p + C_f R_f R_s R'_p + R_s L'_p + L_s R'_p) \\ &+ R'_c (L_f L'_p + C_f R_f L_s R'_p + C_f L_f R_s R'_p + C_f R_f R_s L'_p + L_s L'_p) \\ &+ L'_m R'_c (L_f + R_f R_s C_f + C_f R_f R'_p + L_s + L'_p), \end{aligned} \tag{4.10}$$

$$\begin{aligned} b_3 =& L'_m (L_f L'_p + C_f R_f L_s R'_p + C_f L_f R_s R'_p + C_f R_f R_s L'_p + L_s L'_p) \\ &+ R'_c (C_f L_f L_s R'_p + C_f R_f L_s L'_p + C_f L_f R_s L'_p) \\ &+ L'_m R'_c (R_f L_s C_f + L_f R_s C_f + C_f R_f L'_p + C_f L_f R'_p), \end{aligned} \tag{4.11}$$

$$\begin{aligned} b_4 =& L'_m (C_f L_f L_s R'_p + C_f R_f L_s L'_p + C_f L_f R_s L'_p) \\ &+ R'_c (C_f L_f L_s L'_p) \\ &+ L'_m R'_c (L_f L_s C_f + C_f L_f L'_p), \end{aligned} \tag{4.12}$$

$$b_5 = C_f L_f L_s L'_p L'_m. \tag{4.13}$$

The derived transfer function in Equation 4.6 has a fifth-degree polynomial in the denominator and a first-degree polynomial in the numerator. If the resistances are set to zero $R_f = R_s = R'_p = 0$ and the shunt branch representing the core of the transformer is removed by letting $R'_c \to \infty$ and $L'_m \to \infty$, then the transfer function is reduced to the following equation:

$$H_{LCTr} = \frac{1}{s^3 L_f C_f (L_s + L'_p) + s(L_f + L_s + L'_p)}. \tag{4.14}$$

Equation 4.14 is the same transfer function as for the ideal lossless LCL-filter in equation 4.4 but with a series connection of the primary and secondary side leakage inductance.

5. Experimental study

In this chapter, the verification process of the transfer function derived for the LC-filter and transformer model in Chapter 4 is presented. The derived transfer function is evaluated with simulations and experimental investigations. For the experimental verification, a test bench has been developed based on the same types of components as at the Söderfors test site. The material in this chapter is from **Paper III**.

5.1 Method

The transfer function in Equation 4.6 is evaluated with simulations in LTspice and by experimental trials on the corresponding electrical system in the form of a test bench. In the following sections, the system parameters, the simulation model and the experimental setup are presented.

5.1.1 System parameters

The same system parameters are used in the simulation and the analytical solution of the system. The system parameters are the measured and calculated values for the test bench components. The parameters and their corresponding values are shown in Table 5.1.

The LC-filter is a three-phase Schaffner FN5040-17-83 rated at 7.5 kW. The filter is constructed in such a way that it is not possible to access the neutral point of the capacitors. Therefore, an external capacitor is used in the experiments. The capacitor is an MKP1847H AC filtering metalized polypropylene film capacitor with a rated capacitance of 10 μF.

The transformer is a three-phase TOFS-7,5 rated at 7.5 kVA and 400 V Δ/ 230 V Y with a turns ratio of $n \approx 1.7$. The transformer is supplied by Tramo ETV. For the purpose of the experiments, the transformer has been Y-Y connected. The transformer parameters have been determined with a short-circuit and an open-circuit test from the primary side of the transformer. The tests were performed on all three phases and the results were averaged. The open-circuit test gives the core resistance, R_c, and the magnetizing inductance, L_m. The short-circuit test gives the series equivalent resistance and inductance located to one side of the transformer, which in this case is the primary side of the transformer. For the purpose of the modelling of the system the series equivalent resistance and inductance are divided in half and one half is referred to the secondary side using the turns ratio of the transformer: $R_s = (1.4/2)/n^2 \approx 0.23\,\Omega$ and $L_s = (1.8 \cdot 10^{-3}/2)/n^2 \approx 0.3$ mH.

Table 5.1. *Measured and calculated system parameters for the LC-filter and transformer. The table is from* ***Paper III****.*

Parameter	Value
LC-filter measured values	
Inductance, L_f	2.4 mH
Resistance of inductor, R_f	66 mΩ
Capacitance, C_f	10 μF
Transformer measured values	
Series equivalent resistance	1.4 Ω
Series equivalent inductance	1.8 mH
Core resistance, R_c	8225 Ω
Magnetizing inductance, L_m	9.22 H
Transformer calculated values	
Primary side series resistance, R_p	0.7 Ω
Primary side leakage inductance, L_p	0.9 mH
Secondary side series resistance, R_s	0.23 Ω
Secondary side leakage inductance, L_s	0.3 mH

5.1.2 Simulations

A simulation model of circuit 1 in Figure 4.4 is implemented in LTspice. The system parameters from Section 5.1.1 are used in the simulation model. The voltage source is implemented with an internal resistance of 50 Ω, which corresponds to the internal resistance of the function generator used in the experiments. The output current is compared with the input voltage in the model in order to produce the desired Bode plot. The system is simulated over the frequency range 1 Hz to 4 kHz in steps less than 1 Hz to capture the resonance frequency.

5.1.3 Experimental setup

The experimental study was performed on a test bench with similar types of components as at the Söderfors test site. The experimental setup is shown in Figure 5.1. One phase of the three-phase system is considered. The transformer is short-circuited on the primary side and a function generator is connected to the LC-filter, which represents the AC output voltage from the grid side voltage source converter. The function generator can deliver a sinusoidal voltage with a varying frequency to the system. Measurements of the input voltage and the short-circuit current are performed for certain steps for frequencies from 1 Hz to 4 kHz. The step size of the frequency is reduced around the expected resonance frequency in order to capture the resonance behaviour of the circuit.

The short-circuit current is measured using a current probe Fluke i310s. The current probe is set to measure up to 30 A (10 mV/A). The input voltage

is measured with a differential probe TESTEC TT-SI 902, set to measure up to 140 V with an attenuation ratio of $1/20$. The measurements are logged using a PicoScope 5443A with a measurement frequency of 1 MHz and a hardware resolution of 14 bits. In order to reduce the impact of noise on the measurements, 32 measurements are averaged in the PicoScope software.

A function generator is used to supply the system with an input voltage. The function generator is a GW-instek SFG-1013 with an internal resistance of 50 Ω. The output voltage from the function generator is used as the trigger for the PicoScope in order to improve the data capture.

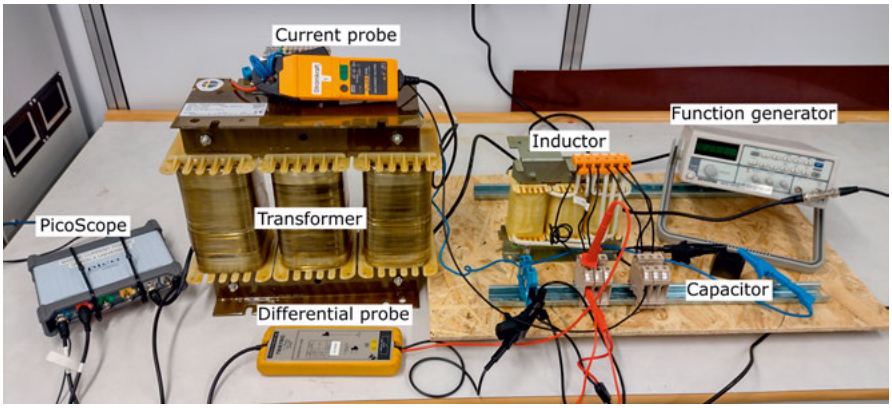

Figure 5.1. Experimental setup. The figure is from **Paper III**.

5.2 Results

The analytical solution, the simulation results, and the measurement results are shown in the Bode plot in Figure 5.2. The analytical solution is the direct solution of the derived transfer function in Equation 4.6. If the magnitude is first considered, it can be observed that the analytical solution and the simulation results overlap almost perfectly. The results from the measurements are up to the resonance peak approximately -1 dB lower than the analytical solution and the simulation results. After the resonance peak, the difference between the measurement data and the analytical solution and the results from the simulation is less than 0.2 dB at the measurements at 3500 Hz and 4000 Hz. The amplitude of the resonance peak is -10.4 dB for the analytical solution and the simulation and -23.8 dB for the experimental data.

The resonance frequency of a lossless LCL-filter with corresponding parameter values to the considered system is approximately 2300 Hz. From Figure 5.2, the resonance peak of the analytical solution and the simulation is observed to occur at approximately $f_0 = 2297$ Hz. The resonance peak in the measurement data occurs between 2290 Hz and 2300 Hz, which means that the

resonance frequency of the measurement data is within 0.4 % of the analytical solution and the simulation results. It can be concluded that the considered system has a resonance frequency equivalent to the resonance frequency of a lossless LCL-filter.

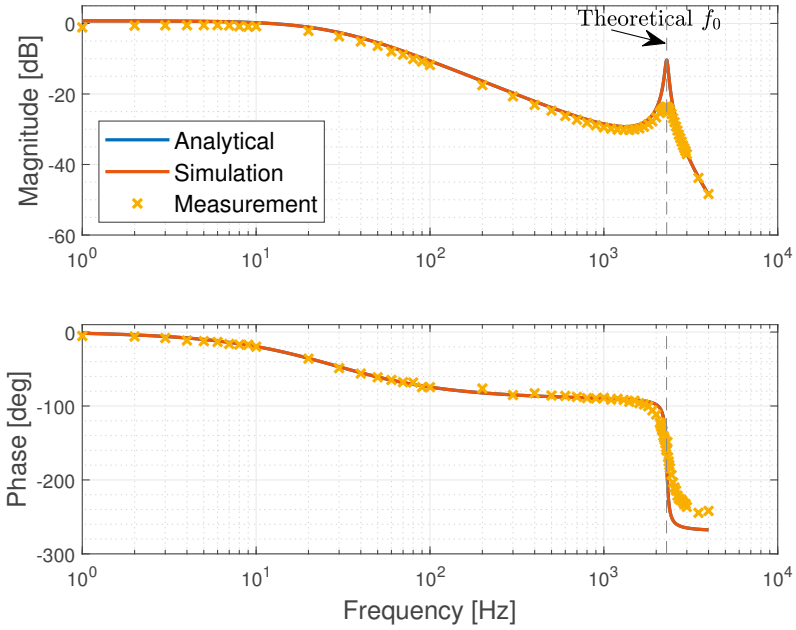

Figure 5.2. Bode plot with the measured data, the analytical solution and the simulation data. Measurement points are marked with an ”x”. The figure is from **Paper III**.

The phase of the analytical solution and the simulation results also overlap almost perfectly, as can be seen in Figure 5.2. The measurement data show a low error when compared with the analytical solution and the simulation results up until the resonance frequency. After the resonance frequency, the measurement data moves towards a value of $-248°$, while the phase of the analytical solution and the simulation settles towards a value of approximately $-268°$.

The experimental results are more damped around the resonance frequency than the analytical solution and the simulation. It is likely that the resistance of cables and connectors has a damping effect on the real system. Since these parts of the system are not included in the model, the possible damping effect of the cables and the connectors is not visible in the analytical solution or the results from the simulation. Other possible explanations for the deviation between the theoretical results and the experimental results are the following:

- Since the average results from the open-circuit and short-circuit tests were used for the transformer parameters, it is possible that the parameters can deviate for a specific phase of the transformer.
- The filter and transformer parameters were determined at the rated frequency. In the experiments, the transfer function was evaluated for a much larger frequency interval.
- Stray capacitances and inductances can possibly influence the experimental results at higher frequencies.
- The currents delivered by the function generator are very small, starting from 40 mA at the lowest frequencies. Small currents are difficult to measure accurately, which can probably give rise to some level of measurement error.

6. Summary and conclusions

Three topics within the grid connection of offshore renewable energy sources have been investigated in the thesis. Firstly, the system perspective has been considered by investigating collection grids and transmission topologies for offshore renewable energy. Secondly, the grid connection system for a marine current energy converter has been investigated. Finally, a specific part of the grid connection system has been studied in detail, and a novel transfer function has been proposed. The thesis is summarized below, and the most important conclusions are presented.

A review of different possible AC and DC collection grids for offshore renewable energy has been presented. Regarding AC collection grids, four main topologies have been identified in the literature:

- The Radial topology
- The Single-sided ring topology
- The Double-sided ring topology
- The Star topology

AC collection grids are the commercial standard. However, DC collection grids can be an interesting option since the losses can be decreased and the components made smaller. Regarding DC grids, two main topologies are identified in the literature: electrically parallel- and series-connected DC collection grids.

The break-even distance between HVAC and HVDC transmission for offshore applications has been investigated. For offshore wind power, different break-even distances are proposed in the literature, depending on the size and distance to the shore of the offshore farm. However, for distances to the shore longer than 50 km to 100 km, HVDC starts to be the preferred solution.

A model for the electrical system of a grid-connected marine current energy converter has been presented. The model is based on an experimental marine current energy converter developed by Uppsala University and deployed in the river Dalälven in Söderfors, Sweden. The grid connection system is based on a B2B converter, where the generator side converter is a 2L-VSC and the grid side converter is a 3L-VSC. The system is bidirectional but in the present study, only the direction of power from the turbine to the grid has been considered. The main purpose of the generator side converter is in this case to maximize the power capture of the turbine, which is achieved with FOC together with an MPPT algorithm. The grid side converter, on the other hand, is supposed to inject the power from the turbine into the distribution grid while maintaining the DC-link voltage. This is achieved with a VOC

method together with a PLL algorithm. The model is implemented in MATLAB/Simulink, and it is shown with simulations that the model of the grid connection system achieves the desired functions. The generator side converter can maximize the power capture of the turbine and the grid side converter can inject the power from the energy converter into the distribution grid while maintaining the DC-link voltage.

Two important parts of a grid connection system are the grid side filter and the power transformer. The purpose of the filter is to remove high-frequency harmonics and the power transformer is supposed to adjust the voltage level of the output voltage from the grid side converter in order to make it suitable for the distribution grid. The frequency response of L-, LC- and LCL-filters has been investigated by using the transfer functions of the filters. A novel transfer function for an LC-filter connected to a power transformer has been proposed. The derived transfer function has been verified with simulations in LTspice and experimental investigations on a test bench. The frequency response of the derived transfer function has been compared with the results from the simulations and the experimental study in terms of a Bode plot. It has been shown that the analytical derived transfer function overlaps almost perfectly with simulations of the corresponding system with regards to both the magnitude and the phase. For the magnitude, the experimental results show a small error of approximately -1 dB compared to the analytical solution up until the resonance frequency. At the resonance frequency, the magnitude for the physical system is -23.8 dB and the magnitude of the analytical solution is -10.4 dB. However, the resonance frequency of the analytical solution and the experimental system occurs at approximately the same frequency of 2297 Hz. After the resonance frequency, the error between the experimental results and analytical solution is less than 0.2 dB.

Regarding the phase, the error between the analytical solution and the experimental results is shown to be small up until the resonance frequency. After the resonance frequency, the phase of the experimental system moves towards -248°, while the phase of the analytical solution and the simulation results settles around -268°.

It can be concluded that the proposed transfer function is able to capture the general behaviour of the frequency response of the system. A possible explanation for the deviation between the theoretical and experimental results is that the resistance of cables and connectors are not included in the theoretical model, which can mean that the physical system is actually more damped than the considered theoretical system. Another possible explanation is measurement errors. The power source used in the experimental study can only deliver small currents. These are difficult to measure, which can give rise to measurement errors.

7. Future work

One interesting area to further investigate is the validity of the simulation model in **Paper I**. This can be achieved by comparing the results from the simulation with data from the Söderfors test site and data from the test bench. Furthermore, it would be useful to use the simulation model to develop improved parameter selection methods for the control system, which could possibly improve the efficiency of the system.

The simulation model could also be used in the DC and AC topologies proposed in **Paper II** to evaluate the stability and efficiency of the different topologies for farms of marine energy converters. Furthermore, since AC and DC collection grids for offshore renewable energy are complicated, large and expensive systems most studies on the subject are based on simulations and theoretical considerations. Therefore, it would also be of interest to experimentally try to evaluate the systems by constructing downscaled models of the topologies.

Another interesting future study would be to use the derived transfer function from **Paper III** in order to improve the control of the grid side converter. This could possibly be achieved by incorporating the transfer function in the control algorithm. The test bench could also be further developed by including a voltage source converter, which would give a more realistic system compared to using a function generator to represent the converter.

8. Summary of papers

In this chapter the papers presented in the thesis are summarized and the contribution of the author is presented.

Paper I

Simulations of the electrical system of a grid connected marine current energy converter

In this paper, a simulation model of the electrical system of a grid-connected marine current energy converter is presented. The marine current energy converter is developed by the division of electricity at Uppsala University and deployed in the river Dalälven in Söderfors, Sweden. The simulation model is implemented in MATLAB/Simulink and is based on the electrical system at the Söderfors test site. The electrical system is based on a PMSG connected to a B2B converter and supplementing components, for example, filters. The generator side converter is a 2L-VSC and the grid side converter is a 3L-VSC. The generator side converter is controlled using FOC with zero d-axis current together with an MPPT algorithm. The generator side converter is controlled using VOC with a PLL method. The generator side converter is connected to the generator via an LC-filter and the grid side converter is connected to the distribution grid via an LC-filter and a power transformer. The implemented simulation model is evaluated with simulations with constant water speed, step changes in the water speed and real water speed data from the test site. It is shown that the implemented control system works as expected. The simulation model is also used to estimate the power losses of the system using steady-state simulations. It is shown that the relative power losses of the system are smallest for a water speed of around $1.30\,\mathrm{m/s}$. The largest contribution to the total losses is from the generator.

The author has developed the simulation model and performed most of the simulations. The author has also written most parts of the paper and been in charge of the final editing and the review process.

The paper is a peer-reviewed conference paper and it was presented orally by the author. The paper is found in the *Proceedings of the 14th European Wave and Tidal Energy Conference (EWTEC)*, 5-9th September 2021, Plymouth, UK.

Paper II

A Review of AC and DC Collection Grids for Offshore Renewable Energy with a Qualitative Evaluation for Marine Energy Resources

This paper presents a review of AC and DC collection grids for offshore renewable energy. The review covers potential AC and DC collection grids topologies, components, operation of components and estimated costs of commercially available components. HVAC and HVDC transmission for offshore applications is also reviewed and the break-even point between the two technologies is investigated with a literature review. Based on the review, five DC collection grid topologies are proposed and qualitatively evaluated for marine energy sources. The proposed DC collection grid topologies are evaluated for the case when the energy converter is submerged and when the energy converter is placed on a platform or floating. The properties, advantages and disadvantages are qualitatively evaluated for the different cases.

The author has written the major parts of the paper and has been in charge of the final editing and the review process.

The paper has been peer-reviewed and published in *Energies* 2022, 15(16), 5816.

Paper III

Experimental investigation of the frequency response of an LC-filter and power transformer for grid connection

In this paper, a novel transfer function for an LC-filter connected to a power transformer is derived and verified with simulations and experimental investigations. The considered system is the grid connection system of the marine current energy converter at the Söderfors test site. The derived transfer function is compared with simulations in LTspice of the corresponding system and it is shown that the simulation results and the results from a direct solution of the analytical transfer function overlap almost perfectly in a Bode plot with regards to the magnitude and the phase. The experimental study is performed on a test bench with the same type of components as at the Söderfors test site. It is shown that the magnitude of the experimental results is approximately -1 dB more attenuated compared with the theoretical results up until the resonance frequency. At the resonance frequency, the peak of the experimental data is -13.5 dB lower than the theoretical results. However, the resonance frequency occurs at approximately the same frequency for the theoretical model and the experimental system. After the resonance frequency, the error between the experimental and theoretical results is less than 0.2 dB. Regarding the phase, the experimental results show a low error compared with the theoretical results up until the resonance frequency. After the resonance frequency, the phase of the analytical solution and the simulation settle to around -268°, while the experimental results move towards -248°. Multiple possible explanations for

the deviation between the theoretical model and the experimental results are given. Among others, it is noted that the resistance of cables and connectors is not included in the theoretical model, which can mean that the theoretical results are less damped compared with the experimental results.

The author has developed the theoretical model and has been a main contributor in developing the test bench and performing the experimental study. The author has written most parts of the paper.

The paper is submitted to the *International Journal of Electrical Power & Energy Systems, 2023*.

9. Svensk sammanfattning

För att uppnå ett elsystem enbart baserat på förnybara energikällor måste den årliga tillväxten av förnybara energikällor anslutna till elnätet öka markant de närmaste åren. Vind- och solkraft kommer säkerligen att ha en betydande roll, men även havsbaserade energikällor, såsom marin strömkraft (tidvattenkraft) och vågkraft, kan potentiellt ge ett betydande bidrag till ökningen av andelen förnybara energikällor på elnätet. Marin strömkraft och vågkraft har en enorm teoretisk potential globalt men är idag i princip helt outnyttjade.

Två viktiga frågor för havsbaserade energislag är hur den elektriska energin transporteras till land och hur energikällorna ansluts till elnätet. Frågorna är relevanta för alla havsbaserade energislag, men i arbetet som har presenterats i den aktuella avhandlingen har fokus legat på marin strömkraft. En av de första frågor som måste besvaras är hur havsbaserade energikällor är sammankopplade till havs. Det traditionella sättet att konstruera ett elnät till havs är att använda växelström. I litteraturen föreslås primärt fyra olika sätt för att konstruera ett sådant växelströmsnät, varav den så kallade radiella topologin är den vanligaste och enklaste topologin. Ett alternativ till växelström, som i princip inte används idag, är att konstruera ett så kallat likströmsnät. Fördelen med likström är bland annat att förlusterna i systemet kan minskas och att komponenterna potentiellt kan göras mindre i storlek. För liksströmsnät går det att identifiera två primära topologier i litteraturen: elektriskt parallell- och seriekopplade nät.

Oavsett hur det interna nätet i en havbaserad park är konstruerat behöver den elektriska energin överföras till land. För korta avstånd till land kan lämpligen samma teknik användas som i det interna nätet i parken. För längre avstånd till land och för stora parker kan det emellertid vara nödvändigt att öka spänningsnivån för att minska transmissionsförlusterna. Traditionellt har växelström med hög spänning (HVAC) använts, men allteftersom vindkraftparker har blivit större och placerade längre från land har det blivit nödvändigt att använda likström med hög spänning (HVDC). Var gränsen går mellan när det är lämpligt att använda HVAC eller HVDC bestäms av en tekno-ekonomisk utvärdering av det specifika projektet. Generellt gäller att den initiala investeringskostnaden är högre för HVDC jämfört med HVAC, medan kostnaden per extra meter överföringsavstånd är lägre för HVDC. En litteraturöversikt visar att om parken är placerad mer än 50 km till 100 km från land börjar HVDC att betraktas som den mest lämpliga teknologin.

När uppsamlingsnätet ute till havs väl är på plats måste de enskilda energikällorna anslutas till nätet. För förnybara energikällor kräver denna koppling ofta en växelriktare baserad på kraftelektronik. Om till exempel solkraft

tas i beaktande genererar solceller likström, vilket betyder att en växelriktare är nödvändig för att kunna ansluta till ett växelströmsnät. För vindkraft kan det också vara nödvändigt att använda en lösning baserad på kraftelektronik trots att vindkraft genererar växelspänning. Problemet för vindkraft är bland annat att den spänning som genereras varierar väldigt mycket, medan distributionsnätet kräver en mycket stabil spänning. En lösning på det här problemet är att frikoppla generatorn och nätet från varandra genom att använda en kraftelektronisk lösning. En vanlig sådan lösning är att två växelriktare ansluts till varandra med en likströmsledning, vilket kallas ”Back-to-Back” (B2B) växelriktare. Växelriktaren mot generatorn är i en sådan uppsättning ansvarig för att styra generatorn, medan växelriktaren mot nätet är ansvarig för att se till att effekt skickas till det externa elnätet.

Avdelningen för elektricitetslära vid Uppsala Universitet har utvecklat en nätansluten marin strömkraftturbin som är placerad på botten av Dalälven i Söderfors, Sverige. Nätanslutningen vid testanläggningen är baserad på en B2B växelriktarteknologi, såsom presenterad ovan. För att kunna utvärdera hur anläggningen beter sig och interagerar med elnätet är det viktigt att kunna simulera anläggningen. Därför har en simuleringsmodell av nätanslutningen utvecklats. I avhandlingen har det visats genom simuleringar med bland annat vattenhastigheter från testanläggningen att den modell som har implementerats i ett simuleringsprogram har ett önskat beteende.

Det elektriska systemet för nätanslutning som finns i testanläggningen i Söderfors består utöver B2B växelriktaren av flertalet stödkomponenter, bland annat elektriska filter och en transformator. Elektriska filter används för att förbättra kvaliteten på spänningen, medan transformatorer primärt används för att ändra spänningsnivåer på växelspänning. För elektriska filter är det viktigt att studera hur de beter sig för olika frekvenser på spänningar och för detta används ofta ett matematiskt uttryck som kallas överföringsfunktion. För nätanslutningen vid testanläggningen i Söderfors är det elektriska systemet uppbyggt på ett sådant sätt att ett elektriskt filter är anslutet till en transformator som sedan är ansluten till distributionsnätet. För att kunna utvärdera beteendet på det här systemet presenteras i avhandlingen härledningen av en matematisk överföringsfunktion för den här kopplingen samt verifiering av överföringsfunktionen med hjälp av simuleringar och experiment. Det visas att den härledda överföringsfunktionen överensstämmer i princip perfekt med simuleringarna. Den härledda överföringsfunktionen lyckas även fånga det generella beteendet vid en jämförelse med de experimentella resultaten men avvikelsen är något större. En möjlig förklaring till avvikelsen mellan den teoretiska modellen och de experimentella resultaten är att den teoretiska modellen inte innehåller alla delar som finns i det faktiska fysiska systemet. Dessutom är det möjligt att mätfel kan vara en orsak till avvikelsen. Den utrustning som användes i experimenten kan nämligen bara leverera relativt små strömmar, vilka kan vara svåra att mäta.

10. Acknowledgements

Firstly, I would like to thank my main supervisor Karin Thomas for all her support and valuable input on the articles and the licentiate thesis. I am very grateful for her expertise and guidance concerning the research, along with her help with the never-ending range of administrative questions. I would also like to thank my co-supervisor Mats Leijon for all his support, engaging discussions on electricity, as well as his input on my research. Furthermore, I would also like to thank Johan Forslund for all his help with everything regarding the Söderfors test site, contributions to the articles and proofreading. Additionally, I want to thank all my co-authors for all of their contributions to the articles.

I would also like to give a big thanks to Erik Jonasson, Samuel Forsberg, Johannes Hjalmarsson, Carl Flygare, Christoffer Aalhuizen and Md Imran Ullah for proofreading my licentiate thesis. Furthermore, I want to thank all the PhD students and my other colleagues at the Division of Electricity for all of their support.

I would also especially want to give a big thanks to my partner for all of her support.

Finally, I want to thank STandUP for Energy for financing part of this work.

References

[1] "Renewables 2022 Global Status Report," REN21 Secretariat, Tech. Rep., Paris, France, 2022.

[2] "World Energy Outlook 2022," International Energy Agency (IEA), Tech. Rep., Paris, France, Nov. 2022.

[3] "World Energy Resources 2016," World Energy Council, Tech. Rep., London, UK, 2016.

[4] "Ocean Energy Technology Brief 4," International Renewable Energy Agency (IRENA), Tech. Rep., Jun. 2014.

[5] S. Rodrigues, C. Restrepo, E. Kontos, R. Teixeira Pinto, and P. Bauer, "Trends of offshore wind projects," *Renewable and Sustainable Energy Reviews*, vol. 49, pp. 1114–1135, Sep. 2015.

[6] H. Díaz and C. Guedes Soares, "Review of the current status, technology and future trends of offshore wind farms," *Ocean Engineering*, vol. 209, Aug. 2020, Art. no. 107381.

[7] Z. Li, Q. Song, F. An, B. Zhao, Z. Yu, and R. Zeng, "Review on DC transmission systems for integrating large-scale offshore wind farms," *Energy Conversion and Economics*, vol. 2, no. 1, pp. 1–14, Feb. 2021.

[8] R. Teodorescu, P. Rodríguez, and M. Liserre, *Grid converters for photovoltaic and wind power systems*, 3rd ed. Chichester, West Sussex, UK: John Wiley & Sons, 2011.

[9] F. Blaabjerg and K. Ma, "Wind energy systems," *Proceedings of the IEEE*, vol. 105, no. 11, pp. 2116–2131, Nov. 2017.

[10] B. Wu, Y. Lang, N. Zargari, and S. Kouro, *Power conversion and control of wind energy systems*, 1st ed. Hoboken, New Jersey, US: John Wiley & Sons, 2011.

[11] A. Parwal, F. Remouit, Y. Hong, F. Francisco, V. Castellucci, L. Hai, L. Ulvgård, W. Li, E. Lejerskog, A. Baudoin, M. Nasir, M. A. Chatzigiannakou, K. Haikonen, R. Ekström, C. Boström, M. Göteman, R. Waters, O. Svensson, J. Sundberg, M. Rahm, J. Engström, A. Savin, and M. Leijon, "Wave energy research at Uppsala University and the Lysekil research site, Sweden: A status update," in *Proc. 11th European Wave and Tidal Energy Conference (EWTEC)*, Nantes, France, Sep. 6-11, 2015.

[12] S. Apelfröjd, R. Ekström, K. Thomas, and M. Leijon, "A back-to-back 2L-3L grid integration of a marine current energy converter," *Energies*, vol. 8, no. 2, pp. 808–820, Jan. 2015.

[13] S. Apelfröjd, K. Thomas, and M. Leijon, "Experimental verification of a back-to-back 2L-3L grid connection system for a marine current energy converter," in *Proc. 2nd International Conference on Offshore Renewable Energy (CORE2016)*, Glasgow, UK, Sep. 12-14, 2016.

[14] M. Liserre, F. Blaabjerg, and A. Dell'aquila, "Step-by-step design procedure for a grid-connected three-phase PWM voltage source converter," *International Journal of Electronics*, vol. 91, no. 8, pp. 445–460, Aug. 2004.

[15] R. N. Beres, X. Wang, M. Liserre, F. Blaabjerg, and C. L. Bak, "A review of passive power filters for three-phase grid-connected voltage-source converters," *IEEE Journal of Emerging and Selected Topics in Power Electronics*, vol. 4, no. 1, pp. 54–69, Mar. 2016.
[16] Y. Han, M. Yang, H. Li, P. Yang, L. Xu, E. A. A. Coelho, and J. M. Guerrero, "Modeling and stability analysis of LCL-type grid-connected inverters: A comprehensive overview," *IEEE Access*, vol. 7, pp. 114 975–115 001, Aug. 2019.
[17] C. C. Gomes, A. F. Cupertino, and H. A. Pereira, "Damping techniques for grid-connected voltage source converters based on LCL filter: An overview," *Renewable and Sustainable Energy Reviews*, vol. 81, pp. 116–135, Jan. 2018.
[18] S. Lundin, J. Forslund, N. Carpman, M. Grabbe, K. Yuen, S. Apelfröjd, A. Goude, and M. Leijon, "The Söderfors project: Experimental hydrokinetic power station deployment and first results," in *Proc. 10th European Wave and Tidal Energy Conference (EWTEC)*, Aalborg, Denmark, Sep. 2-5, 2013.
[19] E. Segergren, "Direct drive generator for renewable power conversion from water currents," Ph.D. dissertation, Uppsala University, 2005.
[20] K. Thomas, "Low speed energy conversion from marine currents," Ph.D. dissertation, Uppsala University, 2007.
[21] M. Grabbe, "Hydro-kinetic energy conversion: Resource and technology," Ph.D. dissertation, Uppsala University, 2013.
[22] K. Yuen, "System perspectives on hydro-kinetic energy conversion," Ph.D. dissertation, Uppsala University, 2012.
[23] S. Apelfröjd, "Grid connection of permanent magnet generator based renewable energy systems," Ph.D. dissertation, Uppsala University, 2016.
[24] A. Goude, "Fluid mechanics of vertical axis turbines: Simulations and model development," Ph.D. dissertation, Uppsala University, 2012.
[25] J. Forslund, "Studies of a vertical axis turbine for marine current energy conversion: Electrical system and turbine performance," Ph.D. dissertation, Uppsala University, 2018.
[26] E. Lalander, "Hydrokinetic resource assessment: Measurements and models," Ph.D. dissertation, Uppsala University, 2013.
[27] N. Carpman, "Resource characterization and variability studies for marine current power," Ph.D. dissertation, Uppsala University, 2017.
[28] S. Lundin, "Marine current energy conversion," Ph.D. dissertation, Uppsala University, 2016.
[29] G. Quinonez-Varela, G. W. Ault, O. Anaya-Lara, and J. R. McDonald, "Electrical collector system options for large offshore wind farms," *IET Renewable Power Generation*, vol. 1, no. 2, pp. 107–114, Jun. 2007.
[30] R. Srikakulapu and U. Vinatha, "Electrical collector topologies for offshore wind power plants: A survey," in *Proc. 2015 IEEE 10th International Conference on Industrial and Information Systems (ICIIS)*, Peradeniya, Sri Lanka, Dec. 18-20, 2015, pp. 338–343.
[31] P. Lakshmanan, R. Sun, and J. Liang, "Electrical collection systems for offshore wind farms: A review," *CSEE Journal of Power and Energy Systems*, vol. 7, no. 5, pp. 1078–1092, Sep. 2021.
[32] S. Lumbreras and A. Ramos, "Offshore wind farm electrical design: a review,"

Wind Energy, vol. 16, no. 3, pp. 459–473, Apr. 2013.
[33] S. M. Alagab, S. Tennakoon, and C. Gould, "Review of wind farm power collection schemes," in *Proc. 2015 50th International Universities Power Engineering Conference (UPEC)*, Stoke on Trent, UK, Sep. 1-4, 2015.
[34] H. J. Bahirat, B. A. Mork, and H. K. Høidalen, "Comparison of wind farm topologies for offshore applications," in *Proc. 2012 IEEE Power and Energy Society General Meeting*, San Diego, CA, USA, Jul. 22-26, 2012.
[35] S. Lundberg, "Wind farm configuration and energy efficiency studies: series DC versus AC layouts," Ph.D. dissertation, Chalmers University of Technology, 2006.
[36] S. Lundberg, "Evaluation of wind farm layouts," *EPE Journal (European Power Electronics and Drives Journal)*, vol. 16, no. 1, pp. 14–21, Feb. 2006.
[37] "Electricity Ten Year Statement 2014 (ETYS 2014)," National Grid ESO, UK, Tech. Rep., 2014.
[38] "Electricity Ten Year Statement 2015 (ETYS 2015)," National Grid ESO, UK, Tech. Rep., 2015.
[39] N. Holtsmark, H. J. Bahirat, M. Molinas, B. A. Mork, and H. K. Høidalen, "An all-DC offshore wind farm with series-connected turbines: An alternative to the classical parallel AC model?" *IEEE Transactions on Industrial Electronics*, vol. 60, no. 6, pp. 2420–2428, Jun. 2013.
[40] E. Agheb, N. Holtsmark, H. K. Høidalen, and M. Molinas, "High frequency wind energy conversion system for offshore DC collection grid – Part I: Comparative loss evaluation," *Sustainable Energy, Grids and Networks*, vol. 5, pp. 167–176, Mar. 2016.
[41] N. Holtsmark, E. Agheb, M. Molinas, and H. K. Høidalen, "High frequency wind energy conversion system for offshore DC collection grid – Part II: Efficiency improvements," *Sustainable Energy, Grids and Networks*, vol. 5, pp. 177–185, Mar. 2016.
[42] C. G. Dincan, "High power medium voltage DC/DC converter technology for DC wind turbines," Ph.D. dissertation, Aalborg University, 2018.
[43] A. Korompili, Q. Wu, and H. Zhao, "Review of VSC HVDC connection for offshore wind power integration," *Renewable and Sustainable Energy Reviews*, vol. 59, pp. 1405–1414, Jun. 2016.
[44] A. Fernández-Guillamón, K. Das, N. A. Cutululis, and Á. Molina-García, "Offshore wind power integration into future power systems: Overview and trends," *Journal of Marine Science and Engineering*, vol. 7, no. 11, Nov. 2019, Art. no. 399.
[45] G. F. Reed, H. A. A. Hassan, M. J. Korytowski, P. T. Lewis, and B. M. Grainger, "Comparison of HVAC and HVDC solutions for offshore wind farms with a procedure for system economic evaluation," in *Proc. 2013 IEEE Energytech*, Cleveland, OH, USA, May. 21-23, 2013.
[46] A. Alassi, S. Bañales, O. Ellabban, G. Adam, and C. MacIver, "HVDC transmission: Technology review, market trends and future outlook," *Renewable and Sustainable Energy Reviews*, vol. 112, pp. 530–554, Sep. 2019.
[47] J. Green, A. Bowen, L. J. Fingersh, and Y. Wan, "Electrical collection and transmission systems for offshore wind power: Preprint," in *Proc. 2007 Offshore Technology Conference*, Houston, Texas, Apr. 30 - May 3, 2007.

[48] T. Ackermann, “Transmission systems for offshore wind farms,” *IEEE Power Engineering Review*, vol. 22, no. 12, pp. 23–27, Dec. 2002.
[49] P. Bresesti, W. L. Kling, R. L. Hendriks, and R. Vailati, “HVDC connection of offshore wind farms to the transmission system,” *IEEE Transactions on Energy Conversion*, vol. 22, no. 1, pp. 37–43, Mar. 2007.
[50] D. Elliott, K. R. Bell, S. J. Finney, R. Adapa, C. Brozio, J. Yu, and K. Hussain, “A comparison of AC and HVDC options for the connection of offshore wind generation in Great Britain,” *IEEE Transactions on Power Delivery*, vol. 31, no. 2, pp. 798–809, Apr. 2016.
[51] S. Hardy, K. V. Brusselen, S. Hendrix, D. V. Hertem, and H. Ergun, “Techno-economic analysis of HVAC, HVDC and OFAC offshore wind power connections.” in *Proc. 2019 IEEE Milan PowerTech*, Milan, Italy, Jun. 23-27, 2019.
[52] J. Dakic, M. Cheah-Mane, O. Gomis-Bellmunt, and E. Prieto-Araujo, “HVAC transmission system for offshore wind power plants including mid-cable reactive power compensation: Optimal design and comparison to VSC-HVDC transmission,” *IEEE Transactions on Power Delivery*, vol. 36, no. 5, pp. 2814–2824, Oct. 2021.
[53] M. S. Jahan, S. J. Hamim, M. T. I. Bhuiyan, M. J. Abeadin, and M. N. Chowdhury, “Comparative cost analysis of VSC-HVDC and HVAC as transmission system for a 50 MW offshore wind farm in Hatiya island,” in *Proc. 2020 2nd International Conference on Sustainable Technologies for Industry 4.0 (STI)*, Dhaka, Bangladesh, Dec. 19-20, 2020.
[54] B. V. Eeckhout, D. V. Hertem, M. Reza, K. Srivastava, and R. Belmans, “Economic comparison of VSC HVDC and HVAC as transmission system for a 300 MW offshore wind farm,” *European Transactions on Electrical Power*, vol. 20, no. 5, pp. 661–671, Jul. 2010.
[55] J. Dakic, M. Cheah-Mane, O. Gomis-Bellmunt, and E. Prieto-Araujo, “Low frequency AC transmission systems for offshore wind power plants: Design, optimization and comparison to high voltage AC and high voltage DC,” *International Journal of Electrical Power & Energy Systems*, vol. 133, Dec. 2021, Art. no. 107273.
[56] D. Lumbreras, E. Galvez, A. Collado, and J. Zaragoza, “Trends in power quality, harmonic mitigation and standards for light and heavy industries: A review,” *Energies*, vol. 13, no. 21, Nov. 2020, Art. no. 5792.
[57] J. Forslund, K. Thomas, and M. Leijon, “Power and energy needed for starting a vertical axis marine current turbine,” in *Proc. 12th European Wave and Tidal Energy Conference (EWTEC)*, Cork, Ireland, Aug. 27 - Sep. 1, 2017.
[58] M. Büyük, A. Tan, M. Tümay, and K. Ç. Bayindir, “Topologies, generalized designs, passive and active damping methods of switching ripple filters for voltage source inverter: A comprehensive review,” *Renewable and Sustainable Energy Reviews*, vol. 62, pp. 46–69, Sep. 2016.
[59] C. Zhang, T. Dragicevic, J. C. Vasquez, and J. M. Guerrero, “Resonance damping techniques for grid-connected voltage source converters with LCL filters – a review,” in *Proc. 2014 IEEE International Energy Conference (ENERGYCON)*, Cavtat, Croatia, May 13-16, 2014, pp. 169–176.
[60] M. Hanif, V. Khadkikar, W. Xiao, and J. L. Kirtley, “Two degrees of freedom

active damping technique for LCL filter-based grid connected PV systems," *IEEE Transactions on Industrial Electronics*, vol. 61, no. 6, pp. 2795–2803, Jun. 2014.

[61] C. R. Paul, *Introduction to electromagnetic compatibility*, 2nd ed. Hoboken, New Jersey, US: John Wiley & Sons, 2006.